AUTOPHAGY
2017, VOL. 13, NO. 8, 1331–1347
https://doi.org/10.1080/15548627.2017.1327509

Taylor & Francis
Taylor & Francis Group

BASIC RESEARCH PAPER

Check for updates

Classical autophagy proteins LC3B and ATG4B facilitate melanosome movement on cytoskeletal tracks

Amrita Ramkumar[a,b,†], Divya Murthy[a,†], Desingu Ayyappa Raja[a,b], Archana Singh[a], Anusha Krishnan[a,b], Sangeeta Khanna[a], Archana Vats[a], Lipi Thukral[a], Pushkar Sharma[c], Sridhar Sivasubbu[a], Rajni Rani[c], Vivek T. Natarajan[a,b], and Rajesh S. Gokhale[a,b,c,d]

[a]CSIR- Institute of Genomics and Integrative Biology, Mathura Road, New Delhi, India; [b]Academy of Scientific and Innovative Research, Rafi Marg, New Delhi, India; [c]National Institute of Immunology, Aruna Asaf Ali Marg, New Delhi, India; [d]Jawaharlal Nehru Center for Advanced Scientific Research, Jakkur, Bangalore, India

ABSTRACT

Macroautophagy/autophagy is a dynamic and inducible catabolic process that responds to a variety of hormonal and environmental cues. Recent studies highlight the interplay of this central pathway in a variety of pathophysiological diseases. Although defective autophagy is implicated in melanocyte proliferation and pigmentary disorders, the mechanistic relationship between the 2 pathways has not been elucidated. In this study, we show that autophagic proteins LC3B and ATG4B mediate melanosome trafficking on cytoskeletal tracks. While studying melanogenesis, we observed spatial segregation of LC3B-labeled melanosomes with preferential absence at the dendritic ends of melanocytes. This LC3B labeling of melanosomes did not impact the steady-state levels of these organelles but instead facilitated their intracellular positioning. Melanosomes primarily traverse on microtubule and actin cytoskeletal tracks and our studies reveal that LC3B enables the assembly of microtubule translocon complex. At the microtubule-actin crossover junction, ATG4B detaches LC3B from melanosomal membranes by enzymatic delipidation. Further, by live-imaging we show that melanosomes transferred to keratinocytes lack melanocyte-specific LC3B. Our study thus elucidates a new role for autophagy proteins in directing melanosome movement and reveal the unconventional use of these proteins in cellular trafficking pathways. Such crosstalk between the central cellular function and housekeeping pathway may be a crucial mechanism to balance melanocyte bioenergetics and homeostasis.

ARTICLE HISTORY
Received 5 August 2016
Revised 3 April 2017
Accepted 3 May 2017

KEYWORDS
autophagy; cytoskeleton; melanosomes; microtubules; trafficking

Introduction

Lysosome-related organelles are unique vesicular compartments that perform specialized functions in diverse cell types.[1] Melanocytes produce pigment-containing organelles, melanosomes, that are routinely transferred to neighboring keratinocytes in human skin.[2-5] While the basal state of melanosome biogenesis and transfer maintains epidermal homeostasis, this process is augmented by ultraviolet radiations to protect cells from photo damage.[4,6,7] Surprisingly, no active pathways for melanosome removal has been thus far identified.[8-10] The only known pathway of melanosome elimination is through the periodic shedding of keratinocytes via tissue cornification and desquamation.[11-13] Several studies over the years have implicated aberrant melanosome turnover to melanoma malignancies.[14,15]

Autophagy has emerged as an important homeostatic process that maintains energetic balance by recycling of damaged organelles.[16-19] During the selective clearance of organelles such as mitochondria, ribosomes and peroxisomes, organelle-specific adaptor proteins initiate assembly of classical autophagic machinery.[20-22] In all these cases, mammalian orthologs of yeast Atg8 are processed by the cell to become autophagosome-associated molecules. As an example, MAP1LC3B/LC3B (microtubule-associated protein 1 light chain 3 β), a small 18-kDa protein of the LC3 family is processed from the cytosol recruited and is present during the entirety of this autophagic process.[23] Several roles for this protein have been assigned including phagophore elongation and closure, cargo recognition, autophagosome maturation and movement.[24-26] LC3-family proteins are processed and modified by conjugation to phosphatidylethanolamine (PE) to generate a membrane-bound LC3-II (16-kDa) form. This modification process of LC3 is catalyzed by ATG4 (autophagy-related 4, cysteine peptidase) along with ATG3 (autophagy-related 3) and ATG7 (autophagy-related 7) ubiquitin-like conjugating and activating enzymes, respectively.[27] The ATG4 protease is also known to detach LC3-II from membranes after its fusion to lysosomes by delipidating the PE chain.[28,29] The presence of LC3 on melanosomes within melanocytes has been reported, however, the functional significance of such localization remains

CONTACT Rajesh S. Gokhale and Vivek T. Natarajan rsg@igib.res.in; rsg@nii.ac.in; tnvivek@igib.in CSIR-Institute of Genomics and Integrative Biology, Mathura Road, Delhi - 110 020, India.
Supplemental data for this article can be accessed on the publisher's website.
[†]Co-first authors.
© 2017 Taylor & Francis

ambiguous. A recent study has attributed autophagic clearance of melanosomes in keratinocytes based on increased LC3 flux.[31] Labeling of organelles with LC3 is not sufficient to indicate autophagic degradation,[32,33] and several noncanonical functions of LC3 are now emerging.[34-36]

In melanocytes, melanosome biogenesis primarily commences at the perinuclear region within melanocytes.[37,38] Melanosome acquires melanogenic enzymes by sequential trafficking that utilizes endosomal machinery.[39-41] The 4 stages of melanosome maturation are characterized by their unique ultrastructural morphology along with melanin content.[3,42] These pigment-containing organelles then migrate on microtubule tracks to reach cell periphery, where they are translocated to actin filaments and are subsequently transferred to neighboring keratinocytes.[37,38] While the molecular machinery involved in actin-mediated melanosome trafficking is well characterized, involving RAB27A (RAB27A, member RAS oncogene family), MLPH (melanophilin) and MYO5A (myosinVA), the motor assembly required for microtubule (MT) movement is less understood.[37] Recent studies have now implicated the role of RAB1A (RAB1A, member RAS oncogene family)[43] and KIF5B (kinesin family member 5B) in the anterograde trafficking of melanosomes on MT tracks through an adaptor protein PLEKHM2/SKIP (pleckstrin homology and RUN domain containing M2).[44] Incidentally, there seems to be redundancy in translocation complexes for organelles, and clusters of motor protein through a variety of protein complexes are proposed to enhance transport processivity.[45-47]

While studying melanogenesis we unexpectedly observed a marked increase in LC3B flux within melanocytes. Microscopy-based quantitative analysis revealed a subset of melanosomal population to be labeled with LC3B, which also showed a distinct spatial pattern. We show that LC3B makes melanosomes competent to move on MT tracks. Remarkably, another autophagic effector protein ATG4B mediates melanosomal crossover to actin filaments by detaching LC3B through delipidation. Our study elucidates a new role of classical autophagic proteins in mediating movement of melanosomes, an important physiological process involved in protecting genomic DNA damage from ultraviolet radiations.

Results

LC3B is not localized on all melanosomes and shows unique spatial distribution within melanocytes

Previous studies indicate presence of the autophagic marker LC3B on melanosomes[30,48] however, the biological significance could not be established and it is not understood whether melanosomes are cleared through the process of selective autophagy.[49] We first examined B16 melanoma cells to investigate the functional aspects of LC3B on these pigment-containing organelles. Immunofluorescence analysis showed a punctate colocalization for LC3B on melanosomes, which is detected by the HMB45 monoclonal antibody that recognizes PMEL/PMEL17 (premelanosome protein) (Fig. 1A). This antibody in an earlier study has been suggested to primarily label immature melanosomes.[50] Analysis of immunofluorescence images showed overlap coefficient (OC) and Pearson correlation coefficient (PCC) of the order of 0.6 (Fig. 1A), suggesting that not all melanosomes were labeled with LC3B. This colocalization could also be replicated in primary melanocytes where pigmented melanosomes could be detected by brightfield microscopy. As shown in Fig. 1B, we observe colocalization pixels for PMEL and LC3B to be present on mature melanosomes. Similar immunolocalization was also observed using TYRP1 (tyrosinase-related protein 1) and LC3B in B16 cells (Fig. S1). We further examined the colocalization of the LC3B presence on melanosomes in B16 cells, by overexpressing GFP-labeled GPR143/OA1 (G protein-coupled receptor 143), MLANA/MART1 (melan-A), and RAB27A constructs separately along with mCherry-LC3B and tracking the movement of the colocalized spots over a period of time by using live imaging. The colinear movement of the 2 fluorophores provided further confidence of LC3B localization on melanosomes. The Pearson correlation coefficient was estimated to be about 0.80 (Fig. 1C, Video S1, S2, S3). GPR143, MLANA and RAB27A have all been reported to predominantly label melanosomes.[51,52] As also noted in other studies, the differences between overlap coefficients of endogenous and overexpression conditions is attributed to the enhanced expression of protein levels due to overexpression. Further, immunogold electron microscopy (IEM) studies showed LC3B to be present on pigmented melanosomes in the ultrathin microsections of B16 cells embedded in LR-white resin (Fig. 1D, Fig. S2). Since the antibody can also detect cytoplasmic LC3B, some puncta can also be seen in the cytoplasm.

Careful examination of ICC images suggested low abundance of LC3B-labeled melanosomes at the dendritic tips (Fig. 1E). Quantitative analysis of many cells revealed that about two-thirds of the melanosomal population in each cell was labeled with LC3B. The remaining 30% of melanosomes in melanocytes did not colocalize with LC3B. We then estimated colocalized and noncolocalized melanosomal pixels within the B16 cells. Toward this, serial z-stack optical sections of ~500 nm of B16 cells were taken from one end of the cell periphery to the other end. We took the XY plane along the Z axis of the cell, thereby encompassing the total XYZ dimension of the cell. The number of colocalized and noncolocalized melanosomal pixels (PMEL and LC3B) after baseline subtraction was estimated for each section individually. The fraction of LC3B and PMEL-positive melanosomes in each grid was estimated and is plotted as a pie chart, which shows a clear enrichment of LC3-labeled melanosomes at the center of the cell for one single cell. We observed similar enrichment in N = 25 cells. The raw data for 5 representative cells have been included in File S1. Fig. 1F shows the image from dendritic tip to cell center and plots the fraction of LC3B and PMEL-positive melanosomes in each grid is represented as a pie chart. This analysis clearly showed enrichment of LC3-labeled melanosomes in the center of the cell and absence at the periphery was observed.

LC3B present on melanosomes is lipidated at the C terminus

To understand whether LC3B on melanosomal membranes corresponds to the classical lipidated form (LC3-II), we transfected N or C terminus mCherry-tagged LC3B expression plasmids along with GPR143-GFP. Membrane-associated

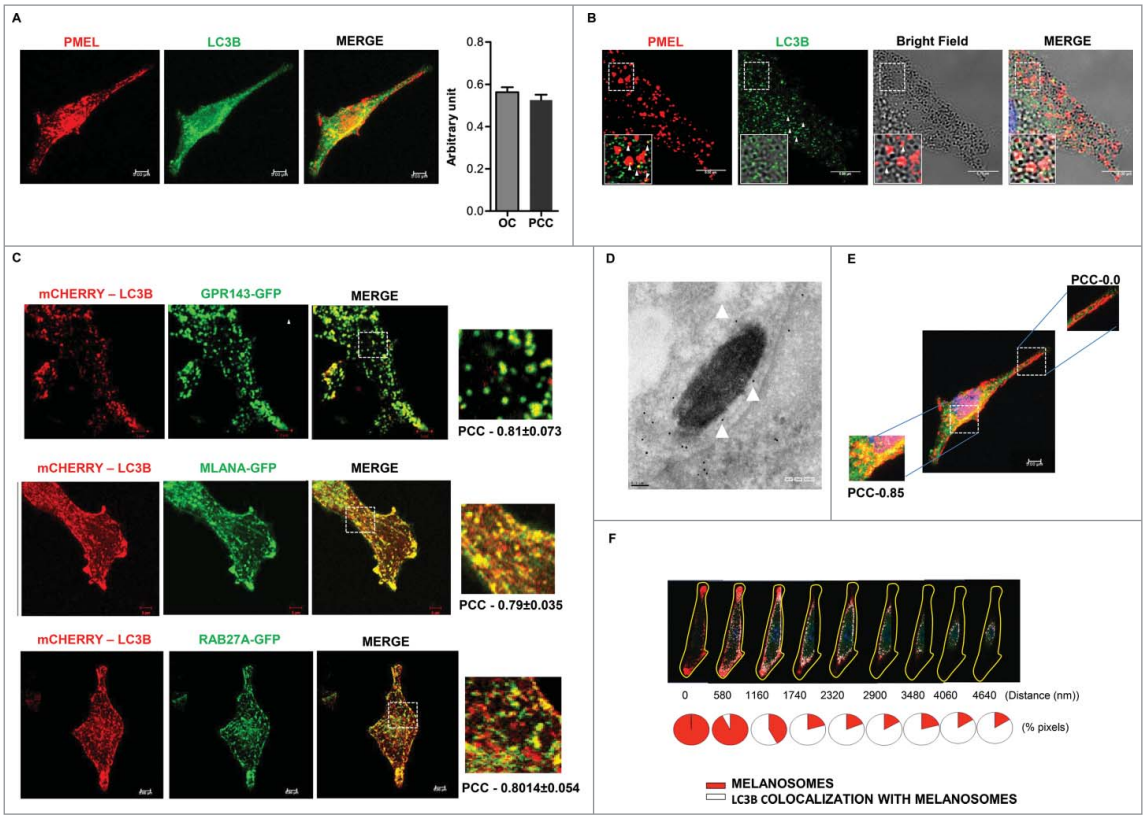

Figure 1. LC3B localization on melanosomes shows spatial distribution in melanocytes. (A) Immunofluorescence micrographs of B16 cells immunostained with melanosome-specific monoclonal antibody HMB45 along with LC3B. Pearson correlation coefficient (PCC) and overlap coefficient (OC) between LC3B and PMEL for the entire cell were calculated (n > 10). Scale bar: 5 μm. (B) Immunofluorescence micrographs of pigmented primary human melanocyte cells immunostained with PMEL and LC3B. Melanosomes were detected under brightfield microscopy as dark granules of melanin. Overlap between each set in shown in the inset. Scale bar: 5 μm. (C) Live imaging snapshots of mCherry-LC3B coexpressed with melanosomal markers GPR143-GFP, MLANA-GFP and RAB27A-GFP showed a high degree of colocalization. The colocalization was quantified by measuring the Pearson correlation coefficient (PCC) as shown in the inset (n > 10). Scale bar: 5 μm. (D) Immunogold electron microscopy (IEM) studies confirm presence of LC3B on melanosomes. High magnification images of B16 cells immunostained with anti-LC3B antibody (secondary antibody conjugated to 10-nm gold beads) marked by white arrowheads. Scale bar: 100 nm. (E) Immunofluorescence micrograph of B16 cells immunostained with PMEL and LC3B. Pearson correlation coefficient between LC3B and PMEL at the dendrites and cell center is represented in the inset. Spatial distribution for colocalized pixels observed. Scale bar: 5 μm. N > 10. (F) Serial z-sections were imaged using confocal microscopy at approximately 500 nm from the cell periphery to cell center. Quantification of colocalized pixels is plotted as pie chart for each stack. Red represents melanosome pixels devoid of LC3B while white represents LC3B colocalized melanosomal pixels. Increased colocalization of melanosomes and LC3B-II is observed in sections spanning center of the cell. Melanosomes devoid of LC3B were mainly present at the dendritic tips. N > 25.

LC3 requires C-terminal cleavage of cytoplasmic LC3 (LC3-I), followed by phosphatidyethanolamine (PE) modification (LC3-II).[27] LC3B-melanosome colocalization analysis showed discrete punctate spots for N terminus-tagged mCherry-LC3B, while C terminus-tagged LC3B-mCherry showed no colocalization (Fig. 2A). Western blot analysis confirmed expression of both these fusion-proteins and thus absence of colocalization for the C terminus construct indicated processing of LC3B protein from the C terminus end (Fig. S3A). The expression of mutant LC3B where the glycine (G) 120 residue has been replaced by alanine (G120A), which cannot undergo proteolytic cleavage, also failed to localize on melanosomes, supporting the prerequisite of C terminus processing (Fig. 2A). Further confidence for these studies was provided by the biochemical analysis of various melanosomal fractions obtained from sucrose density gradient ultracentrifugation of B16 cellular lysates. Analysis of late melanosomal fraction showed a clear enrichment of 16-kDa band, which corresponds to the PE-conjugated LC3 (LC3-II) (Fig. 2B). Such sedimentation equilibrium studies permits relative enrichment of organelle fractions and the 18-kDa band observed in the early melanosome fraction is due to the presence of other cellular components (Fig. S4), which is also seen by the western blot analysis.

LC3B regulation during pigmentation

In an earlier study, we had developed a pigmentation oscillator wherein the depigmented B16 cells maintained in DMEM medium can slowly (in 10 d) be induced to produce pigment by plating cells at low density[53] (Fig. S5). We examined time-dependent changes in LC3B levels during various days of pigmentation using western blot. While D0 of this cycle showed primarily the 18-kDa band corresponding to LC3-I, formation of LC3B-II (16 kDa) could be seen beginning from D4 (Fig. S6A). Quantitative analysis of LC3B-II expression showed approximately 12-fold increase during D4, D6 and D8 (Fig. S7F). We also simultaneously observed increase in the LC3-I levels. The ratio of LC3B-II to LC3B-I, showed a 2.5-fold increase during pigmentation which suggested increased autophagic flux (Fig. S6B). The cells during pigmentation phase in the oscillator model are not replenished with fresh medium, we therefore wanted to examine whether induction of LC3B is not

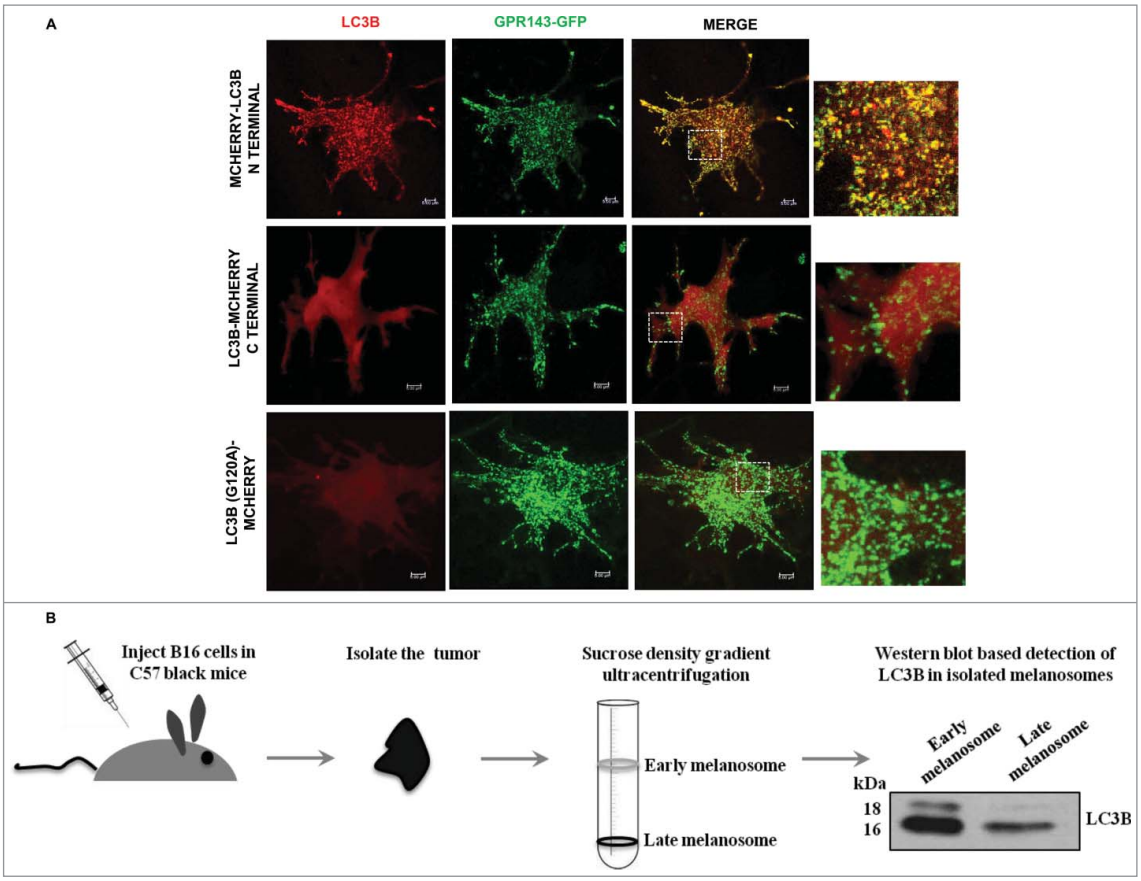

Figure 2. Lipidated LC3B localizes on melanosomes. (A) Live imaging snapshots of B16 cells cotransfected with GPR143-GFP and mCherry-LC3B. While N-terminal-tagged mCherry-LC3B showed localization on melanosomes as observed in the merged image, C-terminal-tagged LC3B-mCherry was absent from melanosomes. The LC3B^{G120A} mutant that is resistant to proteolytic cleavage also failed to colocalize on melanosomes. The localization between GPR143-GFP and mCherry-LC3B for each condition is shown in the insets. Scale bars: 5 μm. (B) Schematic representation for melanosome isolation and purification from tumors using sucrose gradient centrifugation. Western blot analysis of purified melanosome protein fractions shows enrichment of LC3B-II (16 kDa) in both early and late melanosomes that represents the lipidated fraction of LC3B.

an outcome of starvation-induced autophagy.[54] Our earlier observation showed that B16 cells in DMEM-F12 medium even at low density do not undergo a similar process of pigmentation (Fig. S7A, S7B). We thus compared the changes in the expression of LC3B-II under pigmenting and nonpigmenting conditions. Cells cultured in the DMEM and DMEM-F12 media were harvested from the pigmentation phase of D0 to D10. Western blot analysis of LC3B-II showed a 4-fold increase on comparison between the pigmenting and nonpigmenting conditions (Fig S7D, S7E). This suggests that the increased levels of LC3B-II during pigmentation are independent of starvation and may in fact be related to melanogenesis process. Cell cycle analysis also showed no appreciable differences in their overall growth profiles under the 2 culturing conditions (Fig. S7C).

The increase in LC3B levels during pigmentation was rather confounding. While our microscopy studies showed presence of LC3B on melanosomes, the changes in LC3B-II flux could also be a consequence of increased formation of autophagic compartments involving degradation of other cellular cargoes or organelles. Because both autophagosomes and melanosomes can be visualized by EM, we performed quantitative analysis of these 2 organelles during the pigmentation cycle of this oscillator. Ultrastructural analysis showed a clear increase in melanosome numbers with greater number of mature melanosomes (dark granules) during D4, D6, D8 and D10 cells (Fig. S6C, S6D). On the contrary, there were very few double-membrane vesicles indicating no significant differences in the autophagosome numbers (Fig. S6C, S6D), thereby establishing that increase in LC3B flux is not leading to autophagic degradation of melanosomes.

Autophagic pathway analysis during pigmentation

All the above studies suggested that during pigmentation process there are no significant changes in basal autophagy. We then assessed whether the alteration in the autophagy pathway by known pharmacological effectors could impact melanosomes and thereby pigmentation.[55,56] Interestingly, autophagic induction with rapamycin enhanced pigmentation (Fig. S8A, S8B) whereas wortmannin mediated inhibition of autophagy led to a reduction in pigment accumulation (Fig. S8C, S8D). Similar observations have been previously reported for primary melanocytes.[30,57] To carefully examine various stages of autophagic activation, we monitored protein levels of MTOR (mechanistic target of rapamycin), ULK1 (unc-51 like kinase 1) and conjugation complexes. Western blot analysis of ULK1 complexes and ATG3 (autophagy-related 3) showed a slight increase in the expression during the pigmentation cycle. At the same time MTOR, ATG5 (autophagy-related 5), and

ATG12 (autophagy-related 12) showed no differences in protein levels (Fig. S8E). However, we observed a significantly increased expression for BECN1 (Beclin 1, autophagy related) and LC3B in B16 oscillator model (Fig. S8E). This parallels the earlier report, where BECN1 knockdown affects pigmentation. BECN1 has pleotropic roles and thus can affect a variety of cellular functions.[58] Recent studies have identified LC3B presence on variety of nonautophagic vesicles,[35,59] and we therefore further examined this in the context of melanosome biology.

We simultaneously analyzed the localization of LC3B on melanosomes under starvation conditions, wherein activation of the classical autophagy pathway would be induced. After treating B16 cells transfected with GPR143-GFP and mCherry-LC3B, for 8 h with 1X Hank's balanced salt solution (starvation), we observed an increase in the number of autophagosome puncta in starved cells as expected; however, no change in the localization of LC3B on GPR143 melanosomes was observed under these conditions, as accounted by the PCC and OC values. (Fig. S6E). Further, ultrastructural analysis by electron microscopy was performed to assess the maturation status of melanosomes under starvation condition. While we clearly observed an increased number of double-membrane autophogosomes, no significant changes were seen in the numbers of mature (stage III and IV) melanosomes. Together, these data suggested that localization of LC3B on melanosomes remained unaltered on induction of classical autophagy (Fig. S3B, 3C). Similar observations have been reported in MNT-1 cells where induction of autophagosome formation does not alter melanin accumulation within cells.[30]

LC3B does not play a role in biogenesis of melanosomes

Melanosome biogenesis and maturation process require sequential delivery of proteins through vesicular trafficking.[3] Since LC3B flux is significantly enhanced during pigmentation process, we reasoned that LC3B might have a role to play during melanosome formation. We therefore monitored pigmentation after knockdown of LC3B using siRNA. This analysis was performed in B16 cells as well as in primary melanocytes. Interestingly, despite significant reduction in LC3B levels, we observed no change in pigment accumulation in the pelleted cells (Fig. S9A). We then examined expression levels of genes associated with melanosome biogenesis and maturation after LC3B knockdown. Since lysosome biogenesis intersects with the melanosomal pathway,[60] we also included lysosome biogenesis genes during analysis. The central melanogenesis transcription factor *Mitf* (microphthalmia-associated transcription factor)[61] was used as the positive control in this experiment (Fig. S10). Real time-based PCR analysis using B16 mouse melanoma cells showed no significant changes for genes involved in melanosome maturation (*Tyr* [tyrosinase], *Dct* [dopachrome tautomerase] and *Tyrp1* [tyrosinase-related protein 1]) and melanosome biogenesis (such as the *Bloc* [biogenesis of lysosomal organelles complex], *Hps* [Hermansky-Pudlak syndrome] and *Ap-3* [adaptor-related protein complex 3]) complexes (Fig. S9B). Also lysosome biogenesis genes such as *Lamp1* (lysosomal-associated membrane protein 1), *Ctsa* (cathepsin A), *Hexa* (hexosaminidase A) and *Arsa* (arylsulfatase A) also showed no significant changes in their expression levels (Fig. S9B). Western blot analysis for some of the key proteins involved during the pigmentation upon knockdown of LC3B is shown in Fig. S9C. Densitometry quantification, when compared with loading control, showed no significant downregulation for all these proteins (Fig. S9D); however, we observed a slight increase in the levels of TYRP2 and PMEL after LC3B knockdown. We also analyzed the maturation status of melanosomes following LC3B knockdown, by analyzing the ultrastructural details using electron microscopy. We observed no significant changes in the levels of mature (stage III and IV) melanosomes on disruption of endogenous LC3B from B16 cells (Fig. S10D). At the same time, we did not observe accumulation of any vesicles or vacuoles near ER or Golgi, which indicates an absence of any defects in protein trafficking. Next, we monitored the targeting of TYRP1 to PMEL-positive vesicles after LC3B knockdown. The extent of colocalization between TYRP1 and PMEL remained unaltered on endogenous disruption of LC3B. This suggested that the trafficking of key melanogenic protein TYRP1 to melanosomes is not dependent on LC3B (Fig S10E). Together, our studies suggest that LC3B do not play a major role in regulating melanosome biogenesis or maturation.

Knockdown of LC3B affects melanosome positioning within melanocytes

We next performed microscopy analysis of B16 cells after the LC3B knockdown (~65%). To our surprise, we observed a perinuclear clustering of melanosomes and there was a significant absence of melanosomes from the dendritic tips (Fig. 3A). To quantitate the perinuclear aggregation, melanosomes were labeled by the PMEL antibody, tubulin was used to mark the melanocyte cell and DAPI to outline nucleus. Corrected fluorescence intensities were binned into 2 concentric circles that define perinuclear and peripheral region of cells. This analysis was performed with more than 100 cells (Fig. S11). Remarkably, this peculiar aggregation of melanosomes around nucleus could be observed in about 80% of the cells on quantitative analysis (Fig. 3B). Following exogenous expression of siRNA-resistant wild-type (human) mCherry-LC3B in these LC3B-depleted cells, a rescue of the aggregation phenotype could be noted (Fig. 3C, D). Western blot data showed that siRNA did not affect the overexpression of human LC3B within these cells (Fig. 3C). Similar knockdown studies with primary human melanocytes, hyperpigmented B16 cells treated with POMC/α-MSH (pro-opiomelanocortin-α) and with mouse melanocyte (MLANA [melan-A]) cells also showed aggregation of melanosomes at the cell center, both by the brightfield imaging as well as with PMEL immunofluorescence (Fig. 3E, F, Fig. S12). Together, these studies suggested that LC3B might have a role in the intracellular distribution of melanosomes.

To further probe into the defect in melanosome mobility, we analyzed melanosome movement using confocal-based live imaging upon LC3B knockdown. GPR143-GFP transfected cells were treated with control and *Lc3b* siRNA (Fig. 4A, Video S4, S5). Average speed for about 15,000 melanosomes in both control and LC3B knockdown cells was calculated using Volocity software. While the average speed estimated for

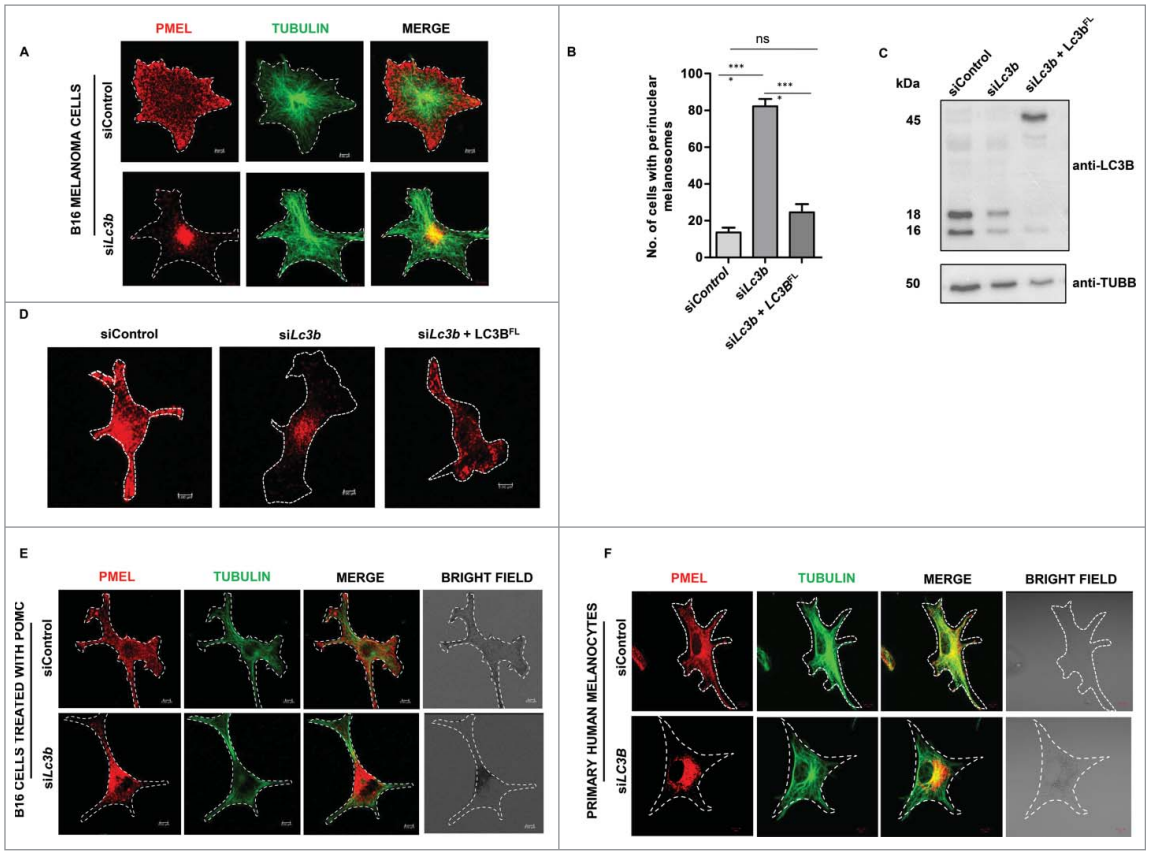

Figure 3. Knockdown of LC3B affects melanosome positioning within melanocytes. (A) Immunofluorescence analysis of melanosome localization as assessed by staining with PMEL and tubulin. Perinuclear aggregation of melanosomes was observed with LC3B knockdown in B16 cells. Both control and experimental data was obtained 48 h post-transfection. Scale bar: 5 μm. (B) Quantification of cells with perinuclear melanosomal aggregation after siRNA-mediated silencing and gene complementation of *Lc3b* in mouse B16 melanoma cells ($n > 100$). Bars represent mean $\pm$ s.e.m. across replicates. (C) Representative blot for the validation of gene knockdown by *Lc3b*-specific siRNA show substantial (65%) downregulation at the protein level (LC3-I:18-kDa and LC3-II:16-kDa) and further complementation with mCherry-tagged LC3B (LC3-I:44-kDa and LC3-II:46-kDa) in the LC3B knockdown background. (D) Immunofluorescence images of B16 cells labeled with PMEL to assess melanosome positioning on LC3B knockdown and rescue. Cells depleted of endogenous LC3B showed perinuclear clustering of melanosomes. On complementation with wild-type human LC3B we observed a rescue in the aggregation phenotype of melanosomes. Scale bar: 5 μm. (E) Immunofluorescence analysis of melanosome localization as assessed by staining with PMEL and tubulin. Perinuclear aggregation of melanosomes was observed on LC3B knockdown in B16 cells hyperpigmented with POMC. Both control and experimental data was obtained 48 h post-transfection. Melanosome clustering could be observed in the brightfield microscopy. Scale bar: 5 μm. (F) Immunofluorescence analysis of melanosome localization as assessed by staining with PMEL and tubulin. Perinuclear aggregation of melanosomes was observed after LC3B knockdown in primary human melanocytes. Both control and experimental data was obtained 48 h post-transfection. Melanosome clustering could be observed in the brightfield microscopy. Scale bar: 5 μm.

melanosome movement in the control set is 0.8 μm/sec, we observed a marked decrease in the speed of melanosomes after LC3B knockdown to about 0.2 μm/sec (Fig. 4B). This data implicated that LC3B knockdown impacts movement of melanosome within melanocytes.

Since LC3 was first identified as a light chain (LC-3) of microtubule-associated protein 1 (MAP1) and 2 (MAP2)[62,63] we wanted to probe whether this melanosome movement defect is not a consequence of microtubule (MT) instability.[64] We analyzed the structural integrity of microtubules after knockdown of the LC3B isoform by using structured illumination microscopy. No structural perturbations were observed on microtubule filaments following LC3B knockdown within B16 cells (Fig. 4C). We then specifically examined the positioning and trafficking of mitochondria within cells that are also known to utilize MT tracks.[65] Mitochondria was labeled using MitoTracker Red and melanosomes were labeled using PMEL antibody. On LC3 knockdown, interestingly, we observed no change in the intracellular distribution of mitochondria, whereas perinuclear clustering of melanosomes was observed within same cells (Fig. 4D). This indicated that the trafficking defect is specific to melanosomes with LC3B knockdown and is not an off-target effect of alteration in MT arrangement. Together, all the data indicated toward a role of LC3B in mediating trafficking of melanosomes within melanocytes.

Role of LC3B in melanosome movement on microtubules

Melanosomes are understood to primarily originate from the center of the cell and traverse on microtubule (MT) tracks to reach the distal ends.[66,67] At the dendritic ends melanosomes crossover to actin filaments that are spatially enriched at the cellular periphery.[37,68] To explain the 2 observations of 1) preferential absence of LC3B-labeled melanosomes from the dendritic tips and 2) perinuclear aggregation of the LC3-depleted melanosomes, we reasoned that LC3B may be crucial for melanosome movement on MT tracks but not on actin filaments. We investigated this hypothesis by examining the localization of melanosomes on cytoskeletal tracks within melanocytes. Immunostaining of melanosomes with tubulin and actin

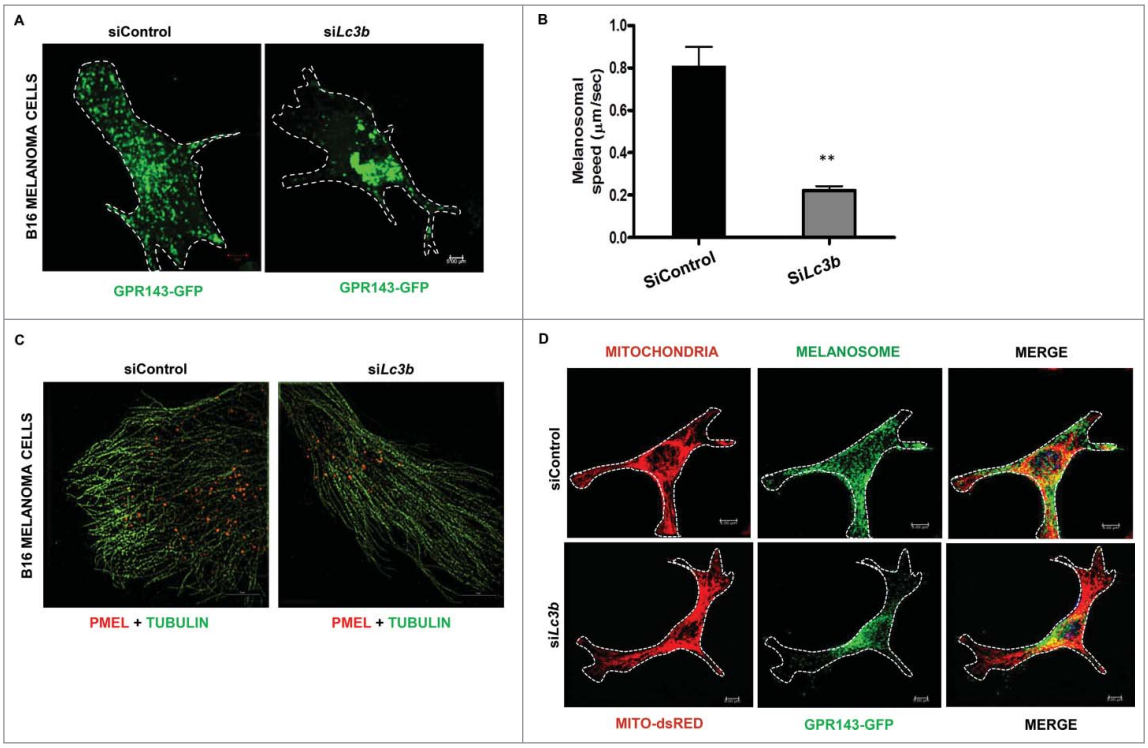

Figure 4. Knockdown of LC3B does not affect microtubule dynamics. (A) Snapshots from live imaging of B16 cells upon knockdown of LC3B. Melanosome dynamics within B16 cells with LC3B knockdown was assessed using confocal-based live-imaging. GPR143-GFP was used to monitor melanosome movement (n > 10). Scale bar: 5 μm. (B) Quantification of average speed for melanosomes (n > 15000) from control and LC3B knockdown set was quantified using Volocity software. Bars represent mean ± s.e.m. across replicates. Significant reduction in speed of melanosome movement is observed following LC3B knockdown. (C) Immunofluorescence analysis of melanosome localization as assessed by staining with PMEL and tubulin using structured illumination microscopy. Perinuclear aggregation of melanosomes was observed after LC3B knockdown in B16 cells. Both control and experimental data were obtained 48 h post-transfection. Structural integrity of microtubules was maintained in both the control and LC3B knockdown data sets. Scale bar: 10 μm. (D) Immunofluorescence micrographs of B16 cells transfected with GPR143-GFP (melanosomes) and MITO-dsRED (mitochondria) in control and LC3B knockdown conditions. While melanosome aggregation at cell center was observed on LC3B knockdown, mitochondrial positioning within cells remained unaffected (n > 10). Scale bar: 5 μm.

showed that melanosomes at the cell center localized on MT whereas at the dendritic tips melanosomes were preferentially present on actin (Fig. 5A). Quantitative analyses of these images were performed by measuring the ratio of colocalized pixels to total number of pixels in different serial sections of the cell. The average percent colocalization pixels between n > 10 cells are plotted in the Flow chart. While similar distribution patterns for PMEL and LC3B, as well as PMEL and tubulin could be seen in Fig. 5B, an exact opposite trend was observed for PMEL and actin. In primary human melanocytes, we performed similar analysis by observing melanosomes using brightfield microscopy. Colocalization analysis showed that melanosomes, which colocalize with actin filaments, show negligible overlap with LC3B and tubulin at the dendritic tips. In contrast, melanosomes enriched on MT tracks at the cell center substantially colocalize with LC3B (Fig. S13).

Further, we examined the effects of various microtubule-disrupting agents on melanosome distribution. While the treatment with nocodazole and vinblastine resulted in perinuclear accumulation of melanosomes, paclitaxel showed melanosome localization at cell periphery (Fig. 5C). Interestingly, this distinct difference in melanosome distribution is concordant with the known action of these inhibitors, where nocodazole and vinblastine interferes with MT polymerization from the plus ends,[69,70] and paclitaxel affects depolymerization of microtubules from the minus ends.[71] We confirmed that these inhibitors did not alter the LC3B expression within the cells (Fig 5D). Live imaging of melanosome dynamics in B16 cells transfected with GPR143-GFP and mCherry-LC3B on addition of nocodazole showed accumulation of LC3-labeled melanosomes in the perinuclear region (Fig. 5E). This indicated that even on distruption of MT tracks, LC3B was associated on melanosomes. Disruption of actin filaments in B16 cells treated with latrunculin B and jasplakinolide showed aggregation around the nucleus. However, here the melanosomes did not form tight perinuclear clustering and many melanosomes could be found on the microtubule tracks (Fig. S14). This phenotype may be due to the involvement of intermediary filaments. Biochemical studies using glutathione-S-transferase-LC3B affinity isolation with purified melanosome lysate also identified tubulin peptides to be among the top hits by mass spectrometric analysis (Fig. S15). All these studies suggest the key role of LC3B in melanosome mobilization on microtubules.

Delipidation activity of ATG4B is crucial for translocation of melanosomes onto actin filaments at dendrites

The presence of LC3B on melanosomes during microtubule movement and its absence during migration on actin filaments suggests that LC3B could be detached from melanosomes at the actin-microtubule junctions. Since LC3B is known to be detached from autophagosome membranes involving delipidation by the ATG4B

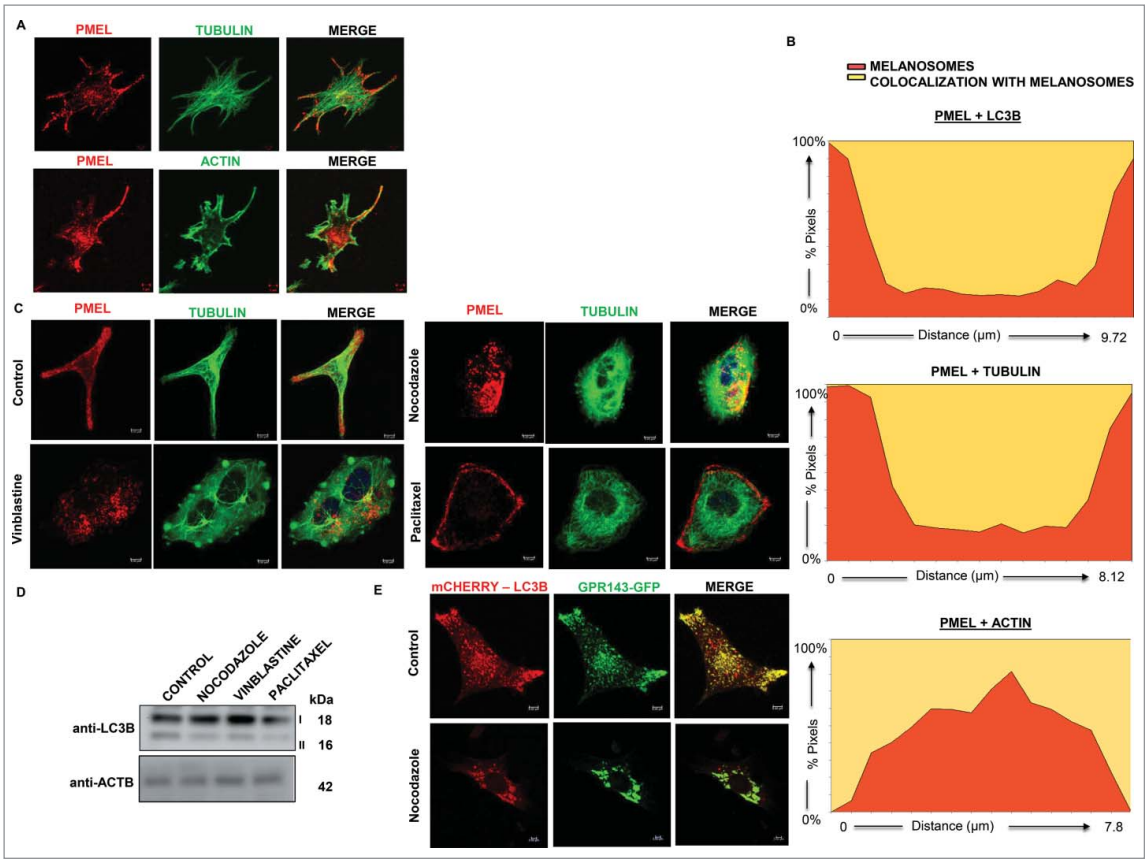

Figure 5. Role of LC3B in melanosome movement on microtubules. (A) Confocal imaging of melanosomes on tubulin and actin networks. Top panels show labeling of melanosomes with PMEL (in red) and tubulin (in green). In the lower panel, melanosomes are labeled with PMEL (in red) and actin tracks (in green) are labeled with phalloidin. Scale bars: 5 μm. (B) Spatial colocalization analysis of melanosome with LC3B, tubulin and actin in B16 cells. Percentage of colocalized pixels for PMEL with LC3B, tubulin and actin is represented as a function of distance from cell surface. Flow plot quantitative measurements show that melanosomes at dendrites are not present on microtubules while those present at the cell center do not colocalize with ACTB. (C) B16 cells treated with modulators of microtubule assembly and disassembly. Treatment with vinblastine (10 μM), nocodazole (0.5 μM) and paclitaxel (10 μM) for 4 h shows disrupted microtubules leading to perturbation in the melanosome dispersion. Scale bar: 5 μm. (D) Western blot analysis of LC3B levels in B16 cells treated with vinblastine (10 μM), nocodazole (0.5 μM) and paclitaxel (10 μM) for 4 h showed no change at the protein level. ACTB was used as normalizing control. (E) Snapshot from live image analysis of B16 cells transfected with GPR143-GFP and mCherry-LC3B on nocodazole treatment (0.5 μM for 3 h). Melanosomes aggregated at the cell center following nocodazole treatment show association with mCherry-LC3B. Scale bar: 5 μm.

enzyme,[29,72] we probed the ATG4B role in melanosome movement. siRNA depletion of endogenous ATG4B levels showed a perinuclear aggregation of melanosomes (Fig. 6A, B). This aggregation defect was rescued on exogenous complementation with human ATG4B construct. In contrast, the catalytically inactive ATG4B^{C74A} mutant could not rescue the aggregation defect (Fig. 6A, C). We also performed colocalization analysis between melanosomes and LC3B after ATG4B knockdown. While the control set showed a significant colocalization value between PMEL and LC3B, the ATG4B knockdown set showed a decrease in overlap coefficient from 0.65 to 0.23 (Fig. S16A).

Incidentally, it is important to note that ATG4B performs another important function, which is converting pro-LC3 to LC3-I by C-terminal clipping at G120 before lipidation.[73,28] To dissect lipidation and delipidation function of ATG4B, we directly expressed an LC3B-I construct (where amino acids 121 to 125 are deleted [LC3B$^{\Delta 121-125}$]), in B16 cells, which can now undergo lipidation without the requirement for ATG4B.[87] Here, only the delipidation activity will be compromised following knockdown of ATG4B within cells. We first validated localization of truncated LC3B protein on melanosome by coexpression of GPR143-GFP and mCherry-LC3B$^{\Delta 121-125}$ in B16 cells. In the presence of the LC3 delipidation mutant protein, melanosomes showed normal dispersion (Fig. S16B). Transfection of mCherry-LC3B$^{\Delta 121-125}$ in the ATG4B knockdown displayed an accumulation of melanosomes in the intermediate region of the cell and no melanosomes were observed in the dendritic periphery. Staining of actin with phalloidin dye showed complete absence of melanosomes from these filaments (Fig. 6D). In contrast, tubulin staining suggested that melanosomes are localized primarily at the peripheral ends of microtubules (Fig. 6E).

To biochemically substantiate these findings, we isolated melanosomes and examined whether purified ATG4B protein can delipidate LC3B from melanosome membranes. Western blot analysis on in vitro incubation of melanosomes with purified ATG4B protein showed decrease in the LC3B-II protein with concomitant increase in the LC3B-I levels (Fig. 6F, G). This provided strong support to the thesis that delipidation of LC3B is mediated by ATG4B and is essential for translocation onto actin filaments.

Knockdown of LC3B affects melanosome transfer to keratinocytes

In skin, melanosomes are routinely transferred from melanocytes to keratinocytes to perform the crucial biological function

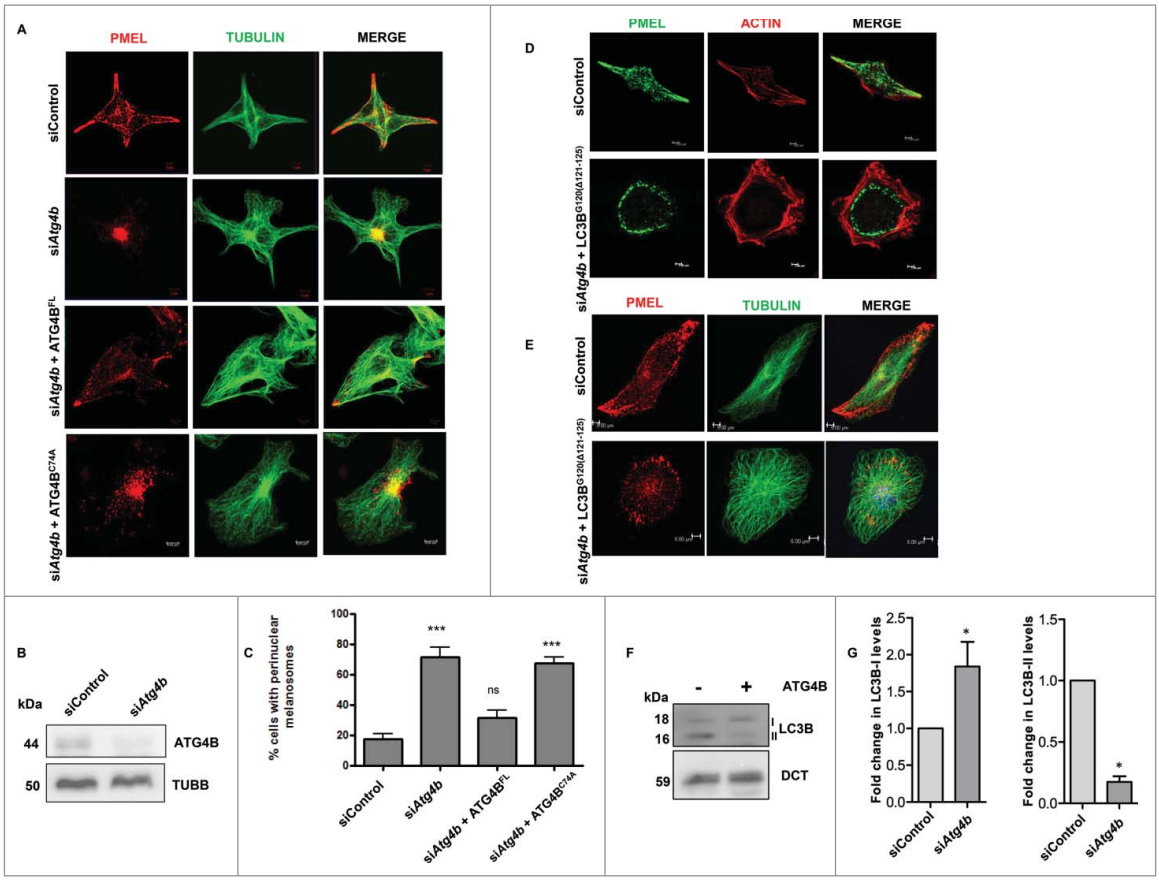

Figure 6. Delipidation activity of ATG4B is crucial for translocation of melanosomes onto actin filaments at dendrites. (A) Immunofluorescence analysis for melanosome localization in B16 cells on ATG4B knockdown. Complementation with siRNA-resistant full-length ATG4B and catalytically inactive ATG4B^{C74A} was performed. While overexpression of full-length ATG4B rescued the melanosome aggregation defect, the ATG4B^{C74A} mutant was unable to rescue the phenotype. Scale bar: 5 μm. (B) Representative western blot for the validation of ATG4B knockdown in B16 cells. (C) Quantitation of cells with perinuclear melanosomal aggregation on siRNA-mediated silencing of ATG4B and on complementation with full length and the ATG4B^{C74A} mutant in mouse B16 melanoma cells (no. of cells analyzed, n>100). Bars represent mean ± s.e.m. across replicates. (D) Immunofluorescence micrographs of B16 cells transfected with mCherry-LC3B$^{\Delta 121-125}$ in a si*Atg4b* background. Melanosomes were stained with PMEL and did not localize on actin filaments (in red) suggesting that delipidation of LC3B-II is essential for actin translocation. Scale bars: 5 μm. (E) Immunofluorescence micrographs of B16 cells transfected with mCherry-LC3B$^{\Delta 121-125}$ in the si*Atg4b* background. Melanosomes were stained with PMEL and were found to be present at the ends of microtubules (tubulin antibody) suggesting hampered movement to the cell periphery. Scale bars: 5 μm. (F) In vitro delipidation assay using recombinant ATG4B was performed on purified melanosomes. Conversion of LC3-II form (16 kDa) to the nonlipidated LC3-I form (18 kDa) was observed, suggesting the role of ATG4B in LC3B delipidation on melanosomes. (G) Densitometric quantification of LC3B-I and LC3B-II protein levels upon ATG4B addition to purified melanosomes shows significant differences. Reduction in LC3-II levels with parallel increase in LC3-I levels was observed (n = 4). Bars represent mean ± s.e.m. across replicates.

of nuclear capping.[74,75] This transfer involves elongation of actin-rich dendrites. Since our studies show that LC3 is absent on melanosomes on actin filaments, the melansomes transferred through this mode should also be devoid of LC3B. We therefore used melanocyte-keratinocyte coculture system.[76] To test whether LC3B-labeled melanosomes are transferred to keratinocytes, we double transfected B16 cells with GPR143-GFP and mCherry-LC3B and examined transfer of melanosomes. Live imaging of these cocultures clearly showed transfer of only GPR143-GFP-labeled melanosomes to keratinocytes (Fig. 7A). Quantitation showed that approximately 90% of the melanosomes in keratinocytes did not contain red fluorescence, suggesting absence of mCherry-LC3B from transferred melanosomes (Fig. 7B). Time-lapse video microscopy revealed dynamic movement for LC3B-devoid melanosomes in keratinocytes, indicating that these organelles move dynamically upon transfer (Video S6). We performed coculture experiments separately with si*Lc3b* and si*Atg4b* in B16 cells. In both these conditions, the number of melanosomes transferred to keratinocytes was drastically (10-fold) reduced as compared with control cells (Fig. S17), highlighting the crucial requirement of LC3B and ATG4B in bringing melanosomes to the dendritic tips of melanocytes.

Discussion

Melanosomes are unique organelles that translocate from their site of biogenesis (melanocytes) to the recipient cells (keratinocytes).[38,77] This transport is essential to maintain genome integrity of keratinocytes and is thus an important aspect of epidermal skin homeostasis.[6,9] In this study, we identify a new role for autophagy proteins LC3B and ATG4B in mediating melanosome movement. By tracking toggled appearance and disappearance of LC3B on melanosomes in 3 distinct steps of their movement, 1) on microtubules (LC3B^{+}) 2) crossover to actin filaments (LC3B^{-}) and 3) transfer to keratinocytes, we establish that LC3B is required for melanosome mobilization on microtubules. Further, we reveal the involvement of the ATG4B protease during its transition from microtubule to actin tracks, which disengages LC3B from melanosome membranes.

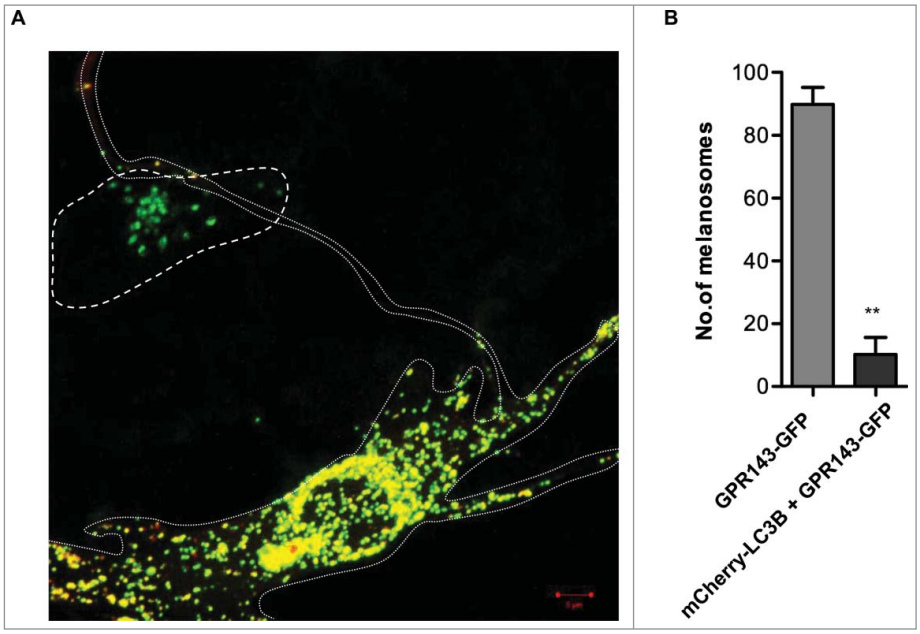

Figure 7. LC3B is crucial for the movement of melanosomes within keratinocytes. (A) B16 cells double transfected with GPR143-GFP and mCherry LC3B were cocultured with keratinocytes (HaCaT) cells for 24 h in the presence of α-MSH (500 nM). Fluorescence analysis of melanosome that were transferred from B16 (dotted line) to HaCaT (dashed line) showed presence of GPR143 protein (green). Remarkably, LC3B-II (red) is not transferred along with these melanosomes. Scale bar: 5 μm. (B) Quantitative analysis was performed using total fluorescence in green (GPR143-GFP) and red+green (GPR143-GFP + mCherry-LC3B) of melanosomes transferred to HaCaT cells from double-transfected B16 cells and it revealed the presence of only GPR143-GFP melanosomes that are devoid of mCherry-LC3B. Bars represent mean $\pm$ s.e.m. across replicates (n $>$ 100).

Thus, the transferred melanosomes to keratinocytes mediated through the actin-rich dendrites therefore lack the melanocyte-specific LC3B.

The intersection of autophagic machinery with melanosome biology is rather intriguing. Classically, LC3B labeling of other organelles has been shown to target them to autophagosomes and this turnover is important to maintain cellular homeostasis.[26] However, recent studies have identified LC3B presence on membraneous compartments that are not targeted for lysosomal degradation.[35] For example, LC3 labeling increases yeast ACB1 (whose mammalian ortholog is DBI [diazepam-binding inhibitor]) and cytokine IL1B/IL-1β (interleukin 1 β) secretion, trafficking of CTSK (cathepsin K) enriched vesicles during osteoclast maturation or during LC3 associated phagocytosis.[78-80] The functional significance of these LC3 labeling is not well understood. Based on our study, it is tempting to speculate that LC3 in all previous instances could also be involved in making these vesicles competent for transport on microtubules. We propose that LC3 enables the assembly of microtubule transposon complex by recruitment of kinesin and dynein motor proteins.[81-83] Adaptor proteins such as MAPK8IP1/JIP1 (mitogen-activated protein kinase 8 interacting protein 1), and FYCO1 (FYVE and coiled-coil domain containing 1), mediate the interactions of LC3 with dynein and kinesin proteins, respectively, for autophagosome trafficking. Such interactions take place classically via the LC3-interacting region motif that is recognized by the N-terminal residues of the LC3 protein along with the core Phe52 residue.[84] We propose a model similar to autophagosomes, for LC3-mediated melanosome translocation on MTs. Our studies show that the LC3B-II form is attached to melanosomes through the C-terminal lipid anchor insertion on membranes. The N-terminal domain of LC3B thus is accessible to mediate interactions with other proteins. A recent study reported the role of PLEKHM2 as the adaptor protein that binds to RAB1A on the melanosome membrane and that assists the recruitment of KIF5B to this complex.[44] At this stage it is not clear whether LC3B is also part of this complex. However, multiple translocon complexes are known to drive organelle movement inside the cell.[88]

The perinuclear aggregation of melanosomes observed during LC3 knockdown is a common phenotype observed upon the knockdown of the 3 motor proteins involved in the trafficking of melanosomes; kinesins (for anterograde movement on microtubule tracks),[44] dyneins (for retrograde movement on microtubule tracks)[85] and myosins (for movement on actin filaments).[86] The interplay between the molecular motors with the 2 cytoskeletal tracks is complex and thus the mechanisms for the redistribution of peripheral melanosomes to the center in all previous instances is unclear. We carefully examined whether LC3B knockdown could directly affect microtubule organization. High-resolution imaging showed no perceptible differences in the positioning of other organelles on LC3B knockdown and thereby provided strong confidence to the involvement of LC3B in melanosome movement. The perinuclear clustering appears to be the most favored steady-state organization, on disruption of melanosome trafficking. Analogous to autophagosome, melanosome may also be using LC3 to form complexes with both kinesin and dynein using different adaptors. The detailed mechanism of LC3B-mediated melanosome movement remains to be delineated further. However, with the available data and taking parallels from the role of LC3 on autophagosome movement, we arrive at a plausible model to explain the perinuclear aggregation of melanosome upon silencing of *Lc3b*.

The unusual intermediate melanosome clustering phenotype for ATG4B knockdown provided clues to the role of this protein in directing the trafficking of melanosomes. Biochemical and mutagenic studies revealed ATG4B involved in delipidating LC3B from the melanosome membrane. Together, our study is suggestive of the role of LC3 in the anterograde movement of melanosomes. Characterization of adaptor proteins along with careful reconstitution of kinesin and dynein translocon complexes in future will facilitate complete understanding of LC3B movement of melansosomes on microtubules.

LC3B-mediated melanosome mobilization and transfer to keratinocytes could be argued to be an indirect mode of cellular clearance. Melanosomes in keratinocytes are sloughed off through the process of epidermal desquamation. Interestingly, melanosome degradation could be a challenge for the cell, since heteropolymeric melanins produced within melanosomes are known to require harsh conditions for degradation.[12] An important question to address in the future would be to delineate how LC3 mechanistically differentiates between the 2 routes—degradation by lysosomal fusion or clearance by vesicular trafficking. Previously, the autophagic effector WIPI1 (WD repeat domain, phosphoinositide interacting 1) has been reported in the transcriptional control of melanosome synthesis. Our study establishes the crucial role of LC3 and ATG4B in melanosome dynamics. The crosstalk between 2 important pathways may be an important facet of maintaining cellular homeostasis. In conclusion, the intersection between the autophagic machinery and organelle trafficking as a mode of cellular clearance and turnover provides a new theme to the understanding of vesicular dynamics.

Materials and methods

Plasmids, antibodies, and reagents

The plasmid for GPR143-EGFP and RAB27A-GFP was a kind gift from Dr. Elena Oancea[90] mCherry-LC3B from Dr. Sovan Sarkar (Massachusetts Institute of Technology). mCherry N1 and mCherry C1 were from Clontech Laboratories (632524, 632523). mCherry-LC3B construct with C- and N-terminal tags were generated using XhoI and HindIII restriction sites. LC3B G120 (Δ120–125) was generated in mCherry-C1 using XhoI-BamHI restriction sites. MLANA-GFP construct was procured from Origene Technologies (MG221327). pStrawberry-ATG4B^{C74A} was procured from Addgene (21076; deposited by Tamotsu Yoshimori). pGEX-6P-ATG4B was generated using EcoRI and SalI restriction sites.

Anti-HMB45 (1:50 for ICC) was obtained from DSS Imagetech (M0634). Antibodies to LC3B (ab51520; 1:1000 for western blot, 1:100 for ICC), tubulin (ab6046; 1:100), SQSTM1/p62 (ab56416; 1:1000), ATG4B (ab70867; 1:1000), mCherry (ab167453; 1:1000), ACTB/-actin (ab8227; 1:5000), LAMP1 (ab24170; 1:1000), DCT/TRP2 (ab74073; 1:1000), PMEL/GP100 (ab137078; 1:1000), MLANA/melan-A (ab51061; 1:500) and BLOC1S4/CNO (ab55038; 1:500) antibodies were purchased from Abcam. ATG5 (12994), ATG12 (4180), ATG3 (3415), BECN1/Beclin1 (3495), MTOR (2983), phosphorylated (p)-MTOR (2974), ULK1 (8054), and phosphorylated (p)-ULK1 (6888) were purchased from Cell Signaling Technology. Secondary antibodies were species-specific antibodies conjugated with either Alexa Fluor 488, 546, 555 or 594, used at a dilution of 1:500 for immunofluorescence (Molecular Probes, Life Technologies A11070, A11010, A21429 and A21203, respectively), or with horseradish peroxidase antibodies used at 1:10,000 for immunoblotting (HRP-labeled anti-mouse secondary antibody [NA931V] and HRP-labeled anti-rabbit secondary antibody [NA934VS] obtained from GE Amersham Health Technologies). To stain for actin filaments, cells were incubated with CytoPainter F-actin Staining Kit - Red Fluorescence (Abcam, 112127) as instructed by the manufacturer. Chemical compounds: Rapamycin (Sigma-Aldrich, R0395–1MG; 5 μM), wortmannin (Sigma-Aldrich, W1628; 200 μM), vinblastine (Sigma-Aldrich, V1377; 5 μM), nocodazole (Sigma-Aldrich, M1404; 0.3 μM) paclitaxel (Sigma-Aldrich, T7402; 10 μM), POMC/α-MSH (Sigma-Aldrich, M4135, 500 nM), jasplakinolide (Sigma-Aldrich, J4580; 2 μM) and latrunculin B (Sigma-Aldrich, L5288; 5 μM).

Cell culture, transfection, and chemical treatments

Cell lines used in this study includes mouse melanoma derived B16-F10 cells (kind gift from Dr. Satyajit Rath, National Institute of Immunology, New Delhi), immortalized keratinocyte HaCaT cell line (kind gift from Dr. Paturu Kondaiah, Indian Institute of Science, Bangalore), primary human melanocytes (Lonza, NHEM-Neo - CC-2504) and MLANA/melan-A (C57BL/6J mouse melanocyte cells; Wellcome Trust Functional Genomics Cell Bank). B16-F10 cells were grown in DMEM-F12 medium (Sigma, D8900) supplemented with heat inactivated 10% fetal bovine serum (FBS; Invitrogen, 10270) at 60% to 80% confluence at 5% CO_2 levels. A bicyclic model was set up in DMEM supplemented with 10% Fetal Bovine Serum by plating 100 cells/cm^2 in replicates and cells were harvested at d 4, 8 and 12. For depigmentation d 12 cells were trypsinized and replated at 10,000 cells/cm^2 and harvested after d 18 and d 20 respectively to complete the 20-day cycle. Cells were transfected at 60% confluency using Lipofectamine 2000 (Invitrogen, 11668019) for expression of plasmid and Dharmafect II (ThermoFisher Scientific, T-2002–03; 1.5 mL) for RNAi oligonucleotides according to the manufacturer's instructions. Transfected cells were analyzed 48 h after transfection. For live imaging, cells were grown in 2-chambered slides (Nunc Lab Tek Chambered Coverglass, 155380).

B16 cells were plated in DMEM-F12 medium at a density of 2×10^5 cells per well of a 6-well plate. Transfection was performed with Dharmafect II reagent (ThermoFisher Scientific, T-2002–03; 1.5 mL) as per manufacturer's protocol. The siRNA concentration used was 100 nM for all siRNAs. Briefly, the cells were incubated with siRNA-Dharmafect II complex for 6 h followed by media change. After 24 h the cells were trypsinised and seeded on coverslips for confocal based analysis. All the siRNAs were purchased from Dharmacon,GE Healthcare Life Sciences. (*Map1Lc3b* mouse; L-040989–01–0005, *MAP1LC3B* Human; L-012846–00–0005, *Atg4b* mouse; L-063865–01–0005, *Mitf* mouse; L-047441–00–0020, *MITF* human; L-008674–00–0020, Non-targeting Pool; D-001810–10–20.)

For cotransfection experiments, 2×10^5 B16 cells were plated in 6-well culture dishes. Twenty-four h later, cells were

transfected using Lipofectamine 2000 transfection reagent with the plasmids mCherry-LC3B and GPR143-EGFP. The total amount of plasmid DNA in each transfection was normalized to 2 μg. 36 h after transfection, cells were lysed as described above for immunoblot analysis or analyzed for confocal-based analysis.

Generation of mutant LC3B vectors

pmCherryC1-LC3B vector encoding human LC3 fused with mCherry was obtained from Dr. Sovan Sarkar. The point mutation for glycine to alanine at position 120 of LC3B ($LC3B^{G120A}$) was created by PCR-based site-directed mutagenesis using the *LC3B* sense primer (5′- GCAGGAGACATTCGCGACAGCCA TGGCTGTG-3′) and *LC3B* antisense primer (5′- CACAGCCA TGGCTGTCGCGAATGTCTCCTGC-3′). The truncation of C-terminal amino acids ($LC3B^{121-125\Delta}$) was created by PCR-based site-directed mutagenesis using the LC3 sense primer (5′- GCCTCGAGCTCGCACCTTCGAACAAAGAG TA-3′) and LC3B antisense primer (5′- GCATGGATCCCCC-GAATGTCTCCTGCGAGGC-3′).

Fractionation of melanosomes by sucrose density gradient centrifugation

Melanosomes were isolated from B16 melanomas induced in C57BL/6 mice, using sucrose density gradient ultracentrifugation. Melanosomes were isolated and purified as described previously.[91] B16 cells were grown to confluence and harvested using 0.1% trypsin-EDTA. The cells were then washed with 10% FBS and pelleted by centrifugation at 1000 g for 5 min at 4°C. Cells were injected in C57 black mice and the B16 melanoma was allowed to grow for 15 to 20 d. The tumor was excised and was washed in homogenization buffer (0.25 M sucrose [Merck, CAS 57–50–1], 10 mM HEPES, 1 mM EDTA, 2% antibiotic and antimycotic [ThermoFisher Scientific, 15240062], pH 7.2) and homogenized with 120 strokes of a Dounce glass homogenizer (Sigma, D8938). The homogenate was then centrifuged at 1000 g for 10 min at 4°C to prepare the post nuclear supernatant. The post nuclear supernatant was collected and separated on a stepwise sucrose density gradient and centrifuged at 100,000 g for 1 h at 4°C in a swing-out rotor (Beckman coulter). The sucrose density gradients comprised 0.25, 0.8, 1.0, 1.2, 1.4, 1.6, 1.8, and 2.0 M sequentially layered with the highest density fraction on the bottom. The stage III and IV melanosomes, which preferentially localized to the high density sucrose fraction, were collected. The isolated fraction was diluted with melanosome wash buffer (0.25 M sucrose, 10 mM HEPES) and centrifuged at 12,000 g for 30 min at 4°C to separate the melanosomal pellet from the sucrose.

Immunofluorescence microscopy

For confocal microscopy and image quantification the cells were plated in 6-well plates on coverslips for d 2, 4, 6, 8, 10. The cells were fixed with 4% paraformaldehyde for 20 min and permeabilized with 0.1% Triton X-100 (Sigma, T9284) for 10 min. 5% normal goat serum (Jackson laboratories, 005–000–121) in phosphate-buffered saline (PBS; HiMedia, M1452) was used for blocking. Staining for HMB45 and MAP1LC3B was done at room temperature for 2 h, rinsed 4 times with PBS-Tween 20 (0.05%; Sigma, P1379), incubated with secondary antibodies produced in mouse or rabbit (diluted 1:500 in 0.5% normal goat serum) for 1 h at room temperature, and washed 4 times with PBS-Tween 20 followed by secondary antibody incubation with Alexa fluor 488 and 568 respectively for 1 h at room temperature. Nuclear staining was performed with SlowFade Gold Antifade with DAPI (Invitrogen, S36938). For quantitative microscopy, the images were acquired at the same settings of the (Detector gain, amplifier offset and pinhole) Ziess LSM 510 Meta confocal microscope (Jena, Germany). Confocal images were captured with a Zeiss 510 or a Zeiss 710 laser-scanning confocal microscope.

RNA extraction and real-time PCR

Isolation of total RNA was performed using Trizol reagent (Invitrogen, 15596–026) and purified using RNeasy Mini Kit (Qiagen, 74104). Quantitative real-time PCR with reverse transcription (qRT-PCR) was performed on a Roche Light Cycler 480 II real-time cycler (ROCHE MOLECULAR DIAGNOSTIC, USA) using the KAPA SYBR FAST qPCR Master Mix (KAPA Biosystems, KM4107) to evaluate transcriptional regulation. Gene-specific primers were obtained from Sigma Aldrich. The relative transcript levels of each target gene were normalized against *Actb* mRNA levels; quantification was performed using the comparative Ct method.

Confocal microscopy, live-cell imaging, and data processing

Fluorescent samples were visualized on a Zeiss LSM 510 or a LSM 710 confocal system (built around a Zeiss Axiovert 200 M inverted microscope, Carl Zeiss, Jena Germany), using a 63X × 1.3 N.A. oil objective. Data were collected as z-stacks with approximately 25 planes and 0.5 to 0.6 μM spacing between each plane. The overlay quantification was performed on Zeiss colocalization parameter by setting the background cut off values with single color channels. The pixels that overlap over and above the background cut-off were considered as colocalized pixels. Individual overlap coefficient and the Pearson coefficient was calculated for all pixels. Merged image was created using the maximum intensity projection software in-built in Zeiss system. Live imaging studies were performed on LSM 710 Zeiss Confocal. Data was collected by capturing 500 continuous frames for approximately 2 min. Video files were created by stitching the different frames together in Zeiss Confocal system. The movement and velocity of melanosomes was evaluated using the *Volocity* software.

Quantitation of perinuclear aggregation of melanosomes

The images acquired using LSM 710 Zeiss Confocal were further processed using ImageJ software. The images were split into 3 channels (RGB). The position of the blue channel (DAPI) was used to mark the cell center. Green channel was used to mark the boundary of the cell and calculate the total area occupied. For final quantification of spatial distribution of

melanosomes, red channel was used. A concentric circle was drawn using the nuclear focal point to bin the cell into 2 effective regions and background (A, peripheral; B, background; C, perinuclear) by taking the cell boundary into account. Next, the mean background intensity was subtracted from the total raw intensity of the cell. The corrected total cell fluorescence was then measured using the following formula:

$$\text{CTCF} = \text{Integrated Density} - (\text{Area of selected cell} \times \text{Mean fluorescence of background readings})$$

The 2 effective areas of the selected region of interest (ROI; A and C) were calculated and the effective fluorescence in respective ROIs was then calculated using the formula:

$$\text{Mean Fluorescence of effective ROI} = \text{Effective Intensity of the area/Effective area}$$

The distribution of fluorescence percentage in each ROI (A/C) was calculated. The loss of fluorescence from the cell periphery was effectively used to calculate the absence from the periphery (also see Fig. S17)

Cell lysis and immunoprecipitation

Mouse B16 melanoma cells were rinsed once with ice-cold PBS and lysed with NP40 lysis buffer (Invitrogen, FNN0021). The soluble fractions of cell lysates were isolated by centrifugation at 13,000 g in a refrigerated microcentrifuge for 15 min. B16 cells transiently expressing mCherry-LC3B were subjected to immunoprecipitation of mCherry using the Catch and release kit from Millipore (17–500). Proteins were eluted with the mCherry tag and resolved on a 15% SDS-PAGE gel.

Cell lysis and western blotting

Cell lysates were prepared using NP40 lysis buffer (Invitrogen, ThermoFisher scientific, FNN0021) reconstituted with protease inhibitor cocktail. Proteins separated by denaturing PAGE were transferred to Immobilon-FL PVDF membranes (Merck Millipore, IPVH00010). Membranes were blocked with 5% milk. Immunoblots were imaged using conventional chemiluminescent immunoblotting. Densitometry was performed using ImageJ.

Cytopainter-based actin staining

For staining of B16 cells with ACTB, the cells were plated on coverslips in 6 well plates. The cells were fixed with 4% paraformaldehyde for 20 min and permeabilized with 0.1% Triton X-100 for 10 min. Normal goat serum (5%) in PBS was used for blocking. Staining with HMB45 was done at room temperature for 2 h, rinsed 4 times with PBS-Tween 20. Next, 100 μL/well of secondary antibody solution diluted in 0.5% BSA (Sigma, A2153) in PBS buffer was added and 100 μL/well 1X Red Fluorescent Phalloidin Conjugate (Abcam, ab112127) working solution. The cells were kept in dark and stained at room temperature for 60 min. The cells were washed 4 times with PBS-Tween 20. Nuclear staining was performed with SlowFade Gold Antifade with DAPI (Invitrogen, S36938). For quantitative microscopy, the images were acquired at the same settings of the (Detector gain, amplifier offset and pinhole) Ziess LSM 510 Meta confocal microscope. Confocal images were captured with a Zeiss 510 or a Zeiss 710 laser-scanning confocal microscope.

Electron microscopy and immunolabeling

B16 cells were trypsinized and fixed with 0.1% glutaraldehyde and 4% paraformaldehyde in 0.1 M sodium cacodylate buffer (pH 7.2) overnight at 4°C. The fixed cells were washed extensively in 0.1 M sodium cacodylate buffer. Next, the samples were sequentially dehydrated in increasing concentration of ethanol. This was followed by sequentially infiltrating the cells with increasing concentrations of LR White resin (Electron Microscopy Sciences, 14381-UC). The cells were then embedded in polymerized LR white resin. Ultrathin sections (70-nm) were cut using a cryoultramicrotome (RMC Powertome PC Arizona, USA), collected on nickel grids (Electron Microscopy Sciences, Cat No- FGF-GA-1500) and treated with 0.1% sodium borohydrate for 15 min. The grids were then blocked with TBSG buffer (1% BSA, 0.1% Tween 20, 0.1% Triton X-100, 3% FBS in 1X TBS buffer [10mM Tris-Cl, pH 7.4, 150 mM NaCl]) for 30 min. The sections were then incubated with anti-LC3B (rabbit polyclonal; Abcam, 51520) overnight at 4°C. After extensive washes with TBS buffer, the grids were incubated with anti-rabbit IgG secondary antibodies coupled to 10-nm colloidal gold particles (Electron Microscopy Sciences, 25108) for 1 h. This was followed by extensive washes in TBS buffer. The grids were then treated with 2% uranyl acetate (Electron Microscopy sciences 22400). The sections were examined in a Tecnai G2 twin transmission electron microscope (FEI, Eindhoven, Netherlands).

Coculture between melanocytes and keratinocytes

Mouse B16 and human HaCaT cells were cocultured at a ratio of 1:3 respectively in DMEM-F12. Briefly, transfected B16 cells were cocultured with untransfected HaCaT cells for 24 h in the presence of POMC/α-MSH to facilitate transfer of melanosomes from melanocytes to the keratinocytes.

Assay for delipidation of LC3-II on melanosomes by ATG4B

Delipidation of LC3B was performed as described in Tanida et al., 2004. Briefly, purified melanosomes were solubilized in NP buffer (0.5% Nonidet P-40 [Thermoscientific, FNN0021], 20 mM potassium phosphate, pH 7.5, 150 mM NaCl). To assay delipidation of LC3B-II, the solubilized late melanosome fraction was treated with 0.5 μg of recombinant ATG4B protein (OriGene, TP300289) and incubated for 2 h at room temperature. To terminate the reaction, Laemmli sample buffer was added to the melanosomal pellet and boiled for 5 min. The total protein was resolved in a 15% SDS-PAGE gel and immunoblotting with an anti-LC3B antibody was done to assay for LC3B delipidation.

Melanin content assay

Melanin content assay was performed as described earlier.[91] Briefly, cells were lysed in 1 N NaOH by heating at 80°C for 2 h and then absorbance was measured at 405 nm. Finally, the melanin content was estimated by interpolating the sample readings on melanin standard curve (μg/ml) obtained with synthetic melanin.

Statistics

All data were analyzed with Prism software (GraphPad, San Diego, CA) using the 2-tailed unpaired Student *t* test. All values are expressed as mean ± s.e.m. Error bars represent standard error mean. Each experiment was replicated at least 3 times as independent biological replicates, as indicated in the figure legends. Differences were considered significant at $P < 0.05$ (*). ** and *** signify $P < 0.01$ and $P < 0.001$ respectively.

Abbreviations

ATG	autophagy related
ATG4B	autophagy-related 4b, cysteine peptidase
BECN1	Beclin 1, autophagy related
DAPI	4′,6-diamidino-2-phenylindole
DMEM	Dulbecco's modified Eagle's medium
DMSO	dimethyl sulfoxide
DNA	deoxyribose nucleic acid
GFP	green flourescent protein
GST	glutathione-S-transferase
GPR143	G protein-coupled receptor 143
ICC	immunocytochemistry
LC3B	microtubule-associated protein 1 light chain 3 β
MT	microtubule
OC	overlap coefficient
PBS	phosphate-buffered saline
PCC	Pearson correlation coefficient
PCR	polymerase chain reaction
PE	phosphatidylethanolamine
PMEL	premelanosome protein
RAB27A	RAB27A, member RAS oncogene family
siRNA	small (or short) interfering RNA
TYRP1	tyrosinase related protein 1

Disclosure of potential conflicts of interest

R.S.G. is the co-founder director on the board of Vyome Biosciences, a biopharmaceutical company in the area of dermatology.

Acknowledgments

We thank Dr. Elena Oancea from Brown University, USA for providing GPR143/OA1 and RAB27A -EGFP construct and Dr. Sovan Sarkar from Massachusetts Institute of Technology, USA for providing mCherry-LC3B construct. We thank Dr. Tarun Kapoor, Rockefeller University, and Dr. K. Natarajan, Jawaharlal Nehru University (JNU) for their valuable suggestions. We also thank Mr. Manish Kumar, microscopy facility and CSIR-IGIB for the infrastructural support through VISION-BSC0403. We thank Dr. Renu Pasricha and TEM facility of National Institute of Biological Sciences (NCBS), Bangalore for their help with IEM experiments.

Funding

ARK and DM are Senior Research Fellows supported by CSIR. LT and AS are supported by DST INSPIRE faculty grant. This work is supported by CSIR grant (TOUCH-BSC0302). We also acknowledge CSIR for institutional support to CSIR-IGIB for imaging facility.

References

[1] Marks MS, Heijnen HF, Raposo G. Lysosome-related organelles: unusual compartments become mainstream. Curr Opin Cell Biol 2013; 25:495-505; PMID:23726022; https://doi.org/10.1016/j.ceb.2013.04.008

[2] Lin JY, Fisher DE. Melanocyte biology and skin pigmentation. Nature 2007; 445:843-50; PMID:17314970; https://doi.org/10.1038/nature05660

[3] Raposo G, Marks MS. Melanosomes–dark organelles enlighten endosomal membrane transport. Nat Rev Mol Cell Biol 2007; 8:786-97; PMID:17878918; https://doi.org/10.1038/nrm2258

[4] Hearing VJ. Biogenesis of pigment granules: a sensitive way to regulate melanocyte function. J Dermatol Sci 2005; 37:3-14; PMID:15619429; https://doi.org/10.1016/j.jdermsci.2004.08.014

[5] Dell'Angelica EC. Melanosome biogenesis: shedding light on the origin of an obscure organelle. Trends Cell Biol 2003; 13:503-6; PMID:14507476; https://doi.org/10.1016/j.tcb.2003.08.001

[6] Maddodi N, Jayanthy A, Setaluri V. Shining light on skin pigmentation: the darker and the brighter side of effects of UV radiation. Photochem Photobiol 2012; 88:1075-82; PMID:22404235; https://doi.org/10.1111/j.1751-1097.2012.01138.x

[7] Virador VM, Muller J, Wu X, Abdel-Malek ZA, Yu ZX, Ferrans VJ, Kobayashi N, Wakamatsu K, Ito S, Hammer JA, et al. Influence of alpha-melanocyte-stimulating hormone and ultraviolet radiation on the transfer of melanosomes to keratinocytes. FASEB J 2002; 16:105-7; PMID:11729101

[8] Kempf VR, Wakamatsu K, Ito S, Simon JD. Imaging, chemical and spectroscopic studies of the methylation-induced decomposition of melanosomes. Photochem Photobiol 2010; 86:765-71; PMID:20331525; https://doi.org/10.1111/j.1751-1097.2010.00721.x

[9] Natarajan VT, Ganju P, Ramkumar A, Grover R, Gokhale RS. Multifaceted pathways protect human skin from UV radiation. Nat Chem Biol 2014; 10:542-51; PMID:24937072; https://doi.org/10.1038/nchembio.1548

[10] Yamaguchi Y, Hearing VJ. Physiological factors that regulate skin pigmentation. Biofactors 2009; 35:193-9; PMID:19449448; https://doi.org/10.1002/biof.29

[11] Boissy RE. Melanosome transfer to and translocation in the keratinocyte. Exp Dermatol 2003; 12(Suppl 2):5-12; PMID:14756517; https://doi.org/10.1034/j.1600-0625.12.s2.1.x

[12] Simon JD, Peles D, Wakamatsu K, Ito S. Current challenges in understanding melanogenesis: bridging chemistry, biological control, morphology, and function. Pigment Cell Melanoma Res 2009; 22:563-79; PMID:19627559; https://doi.org/10.1111/j.1755-148X.2009.00610.x

[13] Abdel-Malek ZA, Kadekaro AL, Swope VB. Stepping up melanocytes to the challenge of UV exposure. Pigment Cell Melanoma Res 2010; 23:171-86; PMID:20128873; https://doi.org/10.1111/j.1755-148X.2010.00679.x

[14] Borovansky J, Mirejovsky P, Riley PA. Possible relationship between abnormal melanosome structure and cytotoxic phenomena in malignant melanoma. Neoplasma 1991; 38:393-400; PMID:1922572

[15] Chen KG, Leapman RD, Zhang G, Lai B, Valencia JC, Cardarelli CO, Vieira WD, Hearing VJ, Gottesman MM. Influence of melanosome dynamics on melanoma drug sensitivity. J Natl Cancer Inst 2009; 101:1259-71; PMID:19704071; https://doi.org/10.1093/jnci/djp259

[16] Rubinsztein DC, Marino G, Kroemer G. Autophagy and aging. Cell 2011; 146:682-95; PMID:21884931; https://doi.org/10.1016/j.cell.2011.07.030

[17] Mizushima N, Ohsumi Y, Yoshimori T. Autophagosome formation in mammalian cells. Cell Struct Funct 2002; 27:421-9; PMID:12576635; https://doi.org/10.1247/csf.27.421

[18] Nakatogawa H, Suzuki K, Kamada Y, Ohsumi Y. Dynamics and diversity in autophagy mechanisms: lessons from yeast. Nat Rev Mol

Cell Biol 2009; 10:458-67; PMID:19491929; https://doi.org/10.1038/nrm2708
[19] Mizushima N, Yoshimori T, Ohsumi Y. The role of Atg proteins in autophagosome formation. Annu Rev Cell Dev Biol 2011; 27:107-32; PMID:21801009; https://doi.org/10.1146/annurev-cellbio-092910-154005
[20] Green DR, Galluzzi L, Kroemer G. Mitochondria and the autophagy-inflammation-cell death axis in organismal aging. Science 2011; 333:1109-12; PMID:21868666; https://doi.org/10.1126/science.1201940
[21] Novak I, Dikic I. Autophagy receptors in developmental clearance of mitochondria. Autophagy 2011; 7:301-3; PMID:21206218; https://doi.org/10.4161/auto.7.3.14509
[22] Farre JC, Burkenroad A, Burnett SF, Subramani S. Phosphorylation of mitophagy and pexophagy receptors coordinates their interaction with Atg8 and Atg11. EMBO Rep 2013; 14:441-9; PMID:23559066; https://doi.org/10.1038/embor.2013.40
[23] Weidberg H, Shvets E, Shpilka T, Shimron F, Shinder V, Elazar Z. LC3 and GATE-16/GABARAP subfamilies are both essential yet act differently in autophagosome biogenesis. EMBO J 2010; 29:1792-802; PMID:20418806; https://doi.org/10.1038/emboj.2010.74
[24] Wild P, McEwan DG, Dikic I. The LC3 interactome at a glance. J Cell Sci 2014; 127:3-9; PMID:24345374; https://doi.org/10.1242/jcs.140426
[25] Slobodkin MR, Elazar Z. The Atg8 family: multifunctional ubiquitin-like key regulators of autophagy. Essays Biochem 2013; 55:51-64; PMID:24070471; https://doi.org/10.1042/bse0550051
[26] Birgisdottir AB, Lamark T, Johansen T. The LIR motif - crucial for selective autophagy. J Cell Sci 2013; 126:3237-47; PMID:23908376
[27] Geng J, Klionsky DJ. The Atg8 and Atg12 ubiquitin-like conjugation systems in macroautophagy. 'Protein modifications: beyond the usual suspects' review series. EMBO Rep 2008; 9:859-64; PMID:18704115; https://doi.org/10.1038/embor.2008.163
[28] Tanida I, Ueno T, Kominami E. Human light chain 3/MAP1LC3B is cleaved at its carboxyl-terminal Met121 to expose Gly120 for lipidation and targeting to autophagosomal membranes. J Biol Chem 2004; 279:47704-10; PMID:15355958; https://doi.org/10.1074/jbc.M407016200
[29] Satoo K, Noda NN, Kumeta H, Fujioka Y, Mizushima N, Ohsumi Y, Inagaki F. The structure of Atg4B-LC3 complex reveals the mechanism of LC3 processing and delipidation during autophagy. EMBO J 2009; 28:1341-50; PMID:19322194; https://doi.org/10.1038/emboj.2009.80
[30] Ho H, Kapadia R, Al-Tahan S, Ahmad S, Ganesan AK. WIPI1 coordinates melanogenic gene transcription and melanosome formation via TORC1 inhibition. J Biol Chem 2011; 286:12509-23; PMID:21317285; https://doi.org/10.1074/jbc.M110.200543
[31] Murase D, Hachiya A, Takano K, Hicks R, Visscher MO, Kitahara T, Hase T, Takema Y, Yoshimori T. Autophagy has a significant role in determining skin color by regulating melanosome degradation in keratinocytes. J Invest Dermatol 2013; 133:2416-24; PMID:23558403; https://doi.org/10.1038/jid.2013.165
[32] Mizushima N, Yoshimori T. How to interpret LC3 immunoblotting. Autophagy 2007; 3:542-5; PMID:17611390; https://doi.org/10.4161/auto.4600
[33] Klionsky DJ, Abeliovich H, Agostinis P, Agrawal DK, Aliev G, Askew DS, Baba M, Baehrecke EH, Bahr BA, Ballabio A, et al. Guidelines for the use and interpretation of assays for monitoring autophagy in higher eukaryotes. Autophagy 2008; 4:151-75; PMID:18188003; https://doi.org/10.4161/auto.5338
[34] Subramani S, Malhotra V. Non-autophagic roles of autophagy-related proteins. EMBO Rep 2013; 14:143-51; PMID:23337627; https://doi.org/10.1038/embor.2012.220
[35] Pimentel-Muinos FX, Boada-Romero E. Selective autophagy against membranous compartments: Canonical and unconventional purposes and mechanisms. Autophagy 2014; 10:397-407; PMID:24419294; https://doi.org/10.4161/auto.27244
[36] Codogno P, Mehrpour M, Proikas-Cezanne T. Canonical and non-canonical autophagy: variations on a common theme of self-eating? Nat Rev Mol Cell Biol 2012; 13:7-12
[37] Hume AN, Seabra MC. Melanosomes on the move: a model to understand organelle dynamics. Biochem Soc Trans 2011; 39:1191-6; PMID:21936787; https://doi.org/10.1042/BST0391191
[38] Wu X, Hammer JA. Melanosome transfer: it is best to give and receive. Curr Opin Cell Biol 2014; 29:1-7; PMID:24662021; https://doi.org/10.1016/j.ceb.2014.02.003
[39] Setaluri V. Sorting and targeting of melanosomal membrane proteins: signals, pathways, and mechanisms. Pigment Cell Res 2000; 13:128-34; PMID:10885669; https://doi.org/10.1034/j.1600-0749.2000.130302.x
[40] Jimbow K, Park JS, Kato F, Hirosaki K, Toyofuku K, Hua C, Yamashita T. Assembly, target-signaling and intracellular transport of tyrosinase gene family proteins in the initial stage of melanosome biogenesis. Pigment Cell Res 2000; 13:222-9; PMID:10952389; https://doi.org/10.1034/j.1600-0749.2000.130403.x
[41] Jimbow K, Gomez PF, Toyofuku K, Chang D, Miura S, Tsujiya H, Park JS. Biological role of tyrosinase related protein and its biosynthesis and transport from TGN to stage I melanosome, late endosome, through gene transfection study. Pigment Cell Res 1997; 10:206-13; PMID:9263327; https://doi.org/10.1111/j.1600-0749.1997.tb00486.x
[42] Hurbain I, Geerts WJ, Boudier T, Marco S, Verkleij AJ, Marks MS, Raposo G. Electron tomography of early melanosomes: implications for melanogenesis and the generation of fibrillar amyloid sheets. Proc Natl Acad Sci U S A 2008; 105:19726-31; PMID:19033461; https://doi.org/10.1073/pnas.0803488105
[43] Ishida M, Ohbayashi N, Maruta Y, Ebata Y, Fukuda M. Functional involvement of Rab1A in microtubule-dependent anterograde melanosome transport in melanocytes. J Cell Sci 2012; 125:5177-87; PMID:22854043; https://doi.org/10.1242/jcs.109314
[44] Ishida M, Ohbayashi N, Fukuda M. Rab1A regulates anterograde melanosome transport by recruiting kinesin-1 to melanosomes through interaction with SKIP. Sci Rep 2015; 5:8238; PMID:25649263; https://doi.org/10.1038/srep08238
[45] Rai A, Pathak D, Thakur S, Singh S, Dubey AK, Mallik R. Dynein Clusters into Lipid Microdomains on Phagosomes to Drive Rapid Transport toward Lysosomes. Cell 2016; 164:722-34; PMID:26853472; https://doi.org/10.1016/j.cell.2015.12.054
[46] Grilli P, Manes L, Maturo A, Carugno F, Camelo M, Governatori N, Rainaldi R, Angelini P, Maggiore D, Salvati B, et al. [Cavernous hemangioma of the small intestine]. G Chir 1989; 10:195-7; PMID:2518555
[47] Erickson RP, Jia Z, Gross SP, Yu CC. How molecular motors are arranged on a cargo is important for vesicular transport. PLoS Comput Biol 2011; 7:e1002032; PMID:21573204; https://doi.org/10.1371/journal.pcbi.1002032
[48] Ho H, Ganesan AK. The pleiotropic roles of autophagy regulators in melanogenesis. Pigment Cell Melanoma Res 2011; 24:595-604; PMID:21777401; https://doi.org/10.1111/j.1755-148X.2011.00889.x
[49] Marks MS. Eating thyself toward the dark side? Pigment Cell Melanoma Res 2009; 22:251-2; PMID:19302107; https://doi.org/10.1111/j.1755-148X.2009.00563.x
[50] Harper DC, Theos AC, Herman KE, Tenza D, Raposo G, Marks MS. Premelanosome amyloid-like fibrils are composed of only golgi-processed forms of Pmel17 that have been proteolytically processed in endosomes. J Biol Chem 2008; 283:2307-22; PMID:17991747; https://doi.org/10.1074/jbc.M708007200
[51] Giordano F, Bonetti C, Surace EM, Marigo V, Raposo G. The ocular albinism type 1 (OA1) G-protein-coupled receptor functions with MART-1 at early stages of melanogenesis to control melanosome identity and composition. Hum Mol Genet 2009; 18:4530-45; PMID:19717472; https://doi.org/10.1093/hmg/ddp415
[52] Bruder JM, Pfeiffer ZA, Ciriello JM, Horrigan DM, Wicks NL, Flaherty B, Oancea E. Melanosomal dynamics assessed with a live-cell fluorescent melanosomal marker. PLoS One 2012; 7:e43465; PMID:22927970; https://doi.org/10.1371/journal.pone.0043465
[53] Natarajan VT, Ganju P, Singh A, Vijayan V, Kirty K, Yadav S, Puntambekar S, Bajaj S, Dani PP, Kar HK, et al. IFN-gamma signaling maintains skin pigmentation homeostasis through regulation of melanosome maturation. Proc Natl Acad Sci U S A 2014; 111:2301-6; PMID:24474804; https://doi.org/10.1073/pnas.1304988111
[54] Wang CW, Klionsky DJ. The molecular mechanism of autophagy. Mol Med 2003; 9:65-76; PMID:12865942

[55] Mizushima N. Methods for monitoring autophagy. Int J Biochem Cell Biol 2004; 36:2491-502; PMID:15325587; https://doi.org/10.1016/j.biocel.2004.02.005
[56] Rodriguez-Enriquez S, Kim I, Currin RT, Lemasters JJ. Tracker dyes to probe mitochondrial autophagy (mitophagy) in rat hepatocytes. Autophagy 2006; 2:39-46; PMID:16874071; https://doi.org/10.4161/auto.2229
[57] Hah YS, Cho HY, Lim TY, Park DH, Kim HM, Yoon J, Kim JG, Kim CY, Yoon TJ. Induction of melanogenesis by rapamycin in human MNT-1 melanoma cells. Ann Dermatol 2012; 24:151-7; PMID:22577264; https://doi.org/10.5021/ad.2012.24.2.151
[58] Wirawan E, Lippens S, Vanden Berghe T, Romagnoli A, Fimia GM, Piacentini M, Vandenabeele P. Beclin1: a role in membrane dynamics and beyond. Autophagy 2012; 8:6-17; PMID:22170155; https://doi.org/10.4161/auto.8.1.16645
[59] Noda T, Yoshimori T. Molecular basis of canonical and bactericidal autophagy. Int Immunol 2009; 21:1199-204; PMID:19737785; https://doi.org/10.1093/intimm/dxp088
[60] Raposo G, Marks MS, Cutler DF. Lysosome-related organelles: driving post-Golgi compartments into specialisation. Curr Opin Cell Biol 2007; 19:394-401; PMID:17628466; https://doi.org/10.1016/j.ceb.2007.05.001
[61] Liu JJ, Fisher DE. Lighting a path to pigmentation: mechanisms of MITF induction by UV. Pigment Cell Melanoma Res 2010; 23:741-5; PMID:20973930; https://doi.org/10.1111/j.1755-148X.2010.00775.x
[62] Kuznetsov SA, Gelfand VI. 18 kDa microtubule-associated protein: identification as a new light chain (LC-3) of microtubule-associated protein 1 (MAP-1). FEBS Lett 1987; 212:145-8; PMID:3803603; https://doi.org/10.1016/0014-5793(87)81574-0
[63] Kouno T, Mizuguchi M, Tanida I, Ueno T, Kanematsu T, Mori Y, Shinoda H, Hirata M, Kominami E, Kawano K. Solution structure of microtubule-associated protein light chain 3 and identification of its functional subdomains. J Biol Chem 2005; 280:24610-7; PMID:15857831; https://doi.org/10.1074/jbc.M413565200
[64] Faller EM, Villeneuve TS, Brown DL. MAP1a associated light chain 3 increases microtubule stability by suppressing microtubule dynamics. Mol Cell Neurosci 2009; 41:85-93; PMID:19233279; https://doi.org/10.1016/j.mcn.2009.02.001
[65] Saxton WM, Hollenbeck PJ. The axonal transport of mitochondria. J Cell Sci 2012; 125:2095-104; PMID:22619228; https://doi.org/10.1242/jcs.053850
[66] Marks MS, Seabra MC. The melanosome: membrane dynamics in black and white. Nat Rev Mol Cell Biol 2001; 2:738-48; PMID:11584301; https://doi.org/10.1038/35096009
[67] Bouzat S, Levi V, Bruno L. Transport properties of melanosomes along microtubules interpreted by a tug-of-war model with loose mechanical coupling. PLoS One 2012; 7:e43599; PMID:22952716; https://doi.org/10.1371/journal.pone.0043599
[68] Wu X, Bowers B, Wei Q, Kocher B, Hammer JA, 3rd. Myosin V associates with melanosomes in mouse melanocytes: evidence that myosin V is an organelle motor. J Cell Sci 1997; 110(Pt 7):847-59; PMID:9133672
[69] Mizuno K, Tolmachova T, Ushakov DS, Romao M, Abrink M, Ferenczi MA, Raposo G, Seabra MC. Rab27b regulates mast cell granule dynamics and secretion. Traffic 2007; 8:883-92; PMID:17587407; https://doi.org/10.1111/j.1600-0854.2007.00571.x
[70] Nilsson H, Rutberg M, Wallin M. Localization of kinesin and cytoplasmic dynein in cultured melanophores from Atlantic cod, Gadus morhua. Cell Motil Cytoskeleton 1996; 33:183-96; PMID:8674138; https://doi.org/10.1002/(SICI)1097-0169(1996)33:3%3c183::AID-CM3%3e3.0.CO;2-C
[71] Panda D, Jordan MA, Chu KC, Wilson L. Differential effects of vinblastine on polymerization and dynamics at opposite microtubule ends. J Biol Chem 1996; 271:29807-12; PMID:8939919; https://doi.org/10.1074/jbc.271.47.29807
[72] Tanida I, Sou YS, Ezaki J, Minematsu-Ikeguchi N, Ueno T, Kominami E. HsAtg4B/HsApg4B/autophagin-1 cleaves the carboxyl termini of three human Atg8 homologues and delipidates microtubule-associated protein light chain 3- and GABAA receptor-associated protein-phospholipid conjugates. J Biol Chem 2004; 279:36268-76; PMID:15187094; https://doi.org/10.1074/jbc.M401461200
[73] Fujita N, Hayashi-Nishino M, Fukumoto H, Omori H, Yamamoto A, Noda T, Yoshimori T. An Atg4B mutant hampers the lipidation of LC3 paralogues and causes defects in autophagosome closure. Mol Biol Cell 2008; 19:4651-9; PMID:18768752; https://doi.org/10.1091/mbc.E08-03-0312
[74] Park HY, Kosmadaki M, Yaar M, Gilchrest BA. Cellular mechanisms regulating human melanogenesis. Cell Mol Life Sci 2009; 66:1493-506; PMID:19153661; https://doi.org/10.1007/s00018-009-8703-8
[75] Byers HR, Maheshwary S, Amodeo DM, Dykstra SG. Role of cytoplasmic dynein in perinuclear aggregation of phagocytosed melanosomes and supranuclear melanin cap formation in human keratinocytes. J Invest Dermatol 2003; 121:813-20; PMID:14632200; https://doi.org/10.1046/j.1523-1747.2003.12481.x
[76] Berens W, Van Den Bossche K, Yoon TJ, Westbroek W, Valencia JC, Out CJ, Marie Naeyaert J, Hearing VJ, Lambert J. Different approaches for assaying melanosome transfer. Pigment Cell Res 2005; 18:370-81; PMID:16162177; https://doi.org/10.1111/j.1600-0749.2005.00263.x
[77] Seiberg M. Keratinocyte-melanocyte interactions during melanosome transfer. Pigment Cell Res 2001; 14:236-42; PMID:11549105; https://doi.org/10.1034/j.1600-0749.2001.140402.x
[78] Bruns C, McCaffery JM, Curwin AJ, Duran JM, Malhotra V. Biogenesis of a novel compartment for autophagosome-mediated unconventional protein secretion. J Cell Biol 2011; 195:979-92; PMID:22144692; https://doi.org/10.1083/jcb.201106098
[79] Malhotra V. Unconventional protein secretion: an evolving mechanism. EMBO J 2013; 32:1660-4; PMID:23665917; https://doi.org/10.1038/emboj.2013.104
[80] Chung YH, Yoon SY, Choi B, Sohn DH, Yoon KH, Kim WJ, Kim DH, Chang EJ. Microtubule-associated protein light chain 3 regulates Cdc42-dependent actin ring formation in osteoclast. Int J Biochem Cell Biol 2012; 44:989-97; PMID:22465708; https://doi.org/10.1016/j.biocel.2012.03.007
[81] Mallik R, Rai AK, Barak P, Rai A, Kunwar A. Teamwork in microtubule motors. Trends Cell Biol 2013; 23:575-82; PMID:23877011; https://doi.org/10.1016/j.tcb.2013.06.003
[82] Hancock WO. Bidirectional cargo transport: moving beyond tug of war. Nat Rev Mol Cell Biol 2014; 15:615-28; PMID:25118718; https://doi.org/10.1038/nrm3853
[83] Kochl R, Hu XW, Chan EY, Tooze SA. Microtubules facilitate autophagosome formation and fusion of autophagosomes with endosomes. Traffic 2006; 7:129-45; PMID:16420522; https://doi.org/10.1111/j.1600-0854.2005.00368.x
[84] Popelka H, Klionsky DJ. Analysis of the native conformation of the LIR/AIM motif in the Atg8/LC3/GABARAP-binding proteins. Autophagy 2015; 11:2153-9; PMID:26565669; https://doi.org/10.1080/15548627.2015.1111503
[85] Byers HR, Yaar M, Eller MS, Jalbert NL, Gilchrest BA. Role of cytoplasmic dynein in melanosome transport in human melanocytes. J Invest Dermatol 2000; 114:990-997; PMID:10771482; https://doi.org/10.1046/j.1523-1747.2000.00957.x
[86] Wu XS, Masedunskas A, Weigert R, Copeland NG, Jenkins NA, Hammer JA. Melanoregulin regulates a shedding mechanism that drives melanosome transfer from melanocytes to keratinocytes. Proc Natl Acad Sci U S A 2012; 10:E2101-210; https://doi.org/10.1073/pnas.1209397109
[87] Tanida I, Ueno T, Kominami E. Human light chain 3/MAP1LC3B is cleaved at its carboxyl-terminal Met121 to expose Gly120 for lipidation and targeting to autophagosomal membranes. J Biol Chem 2004; 279:47704-10; PMID:15355958; https://doi.org/10.1074/jbc.M407016200
[88] Fu MM, Holzbaur EL. Integrated regulation of motor-driven organelle transport by scaffolding proteins. Trends Cell Biol 2014; 24:564-74; PMID:24953741; https://doi.org/10.1016/j.tcb.2014.05.002
[89] Bruder JM, Pfeiffer ZA, Ciriello JM, Horrigan DM, Wicks NL, Flaherty B, Oancea E. Melanosomal dynamics assessed with a live-cell

fluorescent melanosomal marker. PLoS One 2012; 7:e43465; PMID:22927970; https://doi.org/10.1371/journal.pone.0043465

[90] Watabe H, Kushimoto T, Valencia JC, Hearing VJ. Isolation of melanosomes. Curr Protoc Cell Biol 2005; Chapter 3:Unit 3 14; PMID:18228474; https://doi.org/10.1002/0471143030.cb0314s26

[91] Kageyama A, Oka M, Okada T, Nakamura S, Ueyama T, Saito N, Hearing VJ, Ichihashi M, Nishigori C. Down-regulation of melanogenesis by phospholipase D2 through ubiquitin proteasome-mediated degradation of tyrosinase. J Biol Chem 2004; 279:27774-80; PMID:15067002; https://doi.org/10.1074/jbc.M401786200